Published for SISSA by Springer

Received: *June 30, 2025*
Accepted: *September 5, 2025*
Published: *October 21, 2025*

Updated measurement of *CP* violation and polarisation in $B_s^0 \to J/\psi \overline{K}^*(892)^0$ decays

The LHCb collaboration

Full author list at the end of the paper

E-mail: j.wu@cern.ch

Abstract: A time-integrated angular analysis of the decay $B_s^0 \to J/\psi \overline{K}^*(892)^0$, with $J/\psi \to \mu^+\mu^-$ and $\overline{K}^*(892)^0 \to K^-\pi^+$, is presented. The analysis employs a sample of proton-proton collision data collected by the LHCb experiment during 2015–2018 at a centre-of-mass energy of 13 TeV, corresponding to an integrated luminosity of 6 fb^{-1}. A simultaneous maximum-likelihood fit is performed to the angular distributions in bins of the $K^-\pi^+$ mass. This fit yields measurements of the *CP*-averaged polarisation fractions and *CP* asymmetries for the P-wave component of the $K^-\pi^+$ system. The longitudinal and parallel polarisation fractions are determined to be $f_0 = 0.534 \pm 0.012 \pm 0.009$ and $f_\parallel = 0.211 \pm 0.014 \pm 0.005$, respectively, where the first uncertainty is statistical and the second is systematic. The *CP* asymmetries are measured with 3–7% precision and are found to be consistent with zero. These measurements, along with an updated determination of the branching fraction relative to the $B^0 \to J/\psi K^{*0}$ decay, are combined with previous LHCb results, providing the most precise values for these observables to date.

Keywords: B Physics, CP Violation, Hadron-Hadron Scattering, Polarization

ArXiv ePrint: 2506.22090

https://doi.org/10.1007/JHEP10(2025)173

JHEP10(2025)173

Contents

1 Introduction

The study of *CP* violation in the B_s^0 meson system provides crucial tests of the Cabibbo-Kobayashi-Maskawa (CKM) mechanism within the Standard Model (SM) and enables investigation of potential contributions from physics beyond the Standard Model (BSM) [1, 2]. A key observable is the *CP*-violating phase ϕ_s, which arises from the interference between B_s^0 meson decays proceeding directly to a *CP* eigenstate and those occurring after B_s^0–$\overline{B}_s^0$ mixing. Within the SM, neglecting subleading contributions, this phase is predicted to

JHEP10(2025)173

satisfy $\phi_s \approx -2\beta_s$, where $\beta_s = \arg(-V_{ts}V_{tb}^*/V_{cs}V_{cb}^*)$ is related to elements of the CKM matrix [3–5]. Global fits to experimental data, assuming CKM unitarity, provide precise indirect determinations of this phase [6, 7].

Experimentally, ϕ_s is measured directly using decays mediated by the $b \to c\bar{c}s$ transition, with the decay $B_s^0 \to J/\psi\phi$ serving as the benchmark channel. The current world average for the phase measured in $b \to c\bar{c}s$ transitions is $\phi_s^{c\bar{c}s} = -0.052 \pm 0.013\,\text{rad}$ [8]. The excellent theoretical precision of the SM prediction and the relatively clean experimental signature make ϕ_s a powerful probe for BSM effects, which could modify the B_s^0–$\overline{B}_s^0$ mixing amplitude and shift the measured value relative to the SM expectation [9].

However, subleading SM contributions from electroweak loop (penguin) topologies in the $B_s^0 \to J/\psi\phi$ decay process can also induce a phase shift, $\Delta\phi_s$, which complicates the interpretation of the experimental measurement in terms of ϕ_s and thus BSM. The nonperturbative QCD nature of the penguin contributions makes theoretical calculations challenging [10, 11], which can be circumvented using data-driven strategies. One prominent approach, proposed in ref. [12] and further detailed in refs. [13–16], uses *CP* asymmetry measurements of CKM-suppressed $b \to c\bar{c}d$ decays, such as $B_s^0 \to J/\psi\overline{K}^{*0}$ and $B^0 \to J/\psi\rho^0$, to constrain penguin effects in $B_s^0 \to J/\psi\phi$ via approximate SU(3) flavour symmetry. The LHCb collaboration has previously conducted such measurements for $B_s^0 \to J/\psi\overline{K}^*(892)^0$ [17] and $B^0 \to J/\psi\rho(770)^0$[18], using a data sample corresponding to an integrated luminosity of $3\,\text{fb}^{-1}$, collected during 2011–2012 (referred to as Run 1). In addition, the LHCb collaboration also performed an SU(3)-symmetry-based analysis yielding constraints on $\Delta\phi_s$ with uncertainties ranging from 10 to 100 mrad depending on the inputs used [17]. Improving the precision of the $B_s^0 \to J/\psi\overline{K}^{*0}$ parameters is crucial for refining these constraints, especially as the experimental uncertainty on $\phi_s^{c\bar{c}s}$ is reduced.

This paper presents an updated angular analysis of the decay $B_s^0 \to (J/\psi \to \mu^+\mu^-)(\overline{K}^{*0} \to K^-\pi^+)$ using the full dataset collected by the LHCb experiment during the second LHC operational period (Run 2).[1] This dataset corresponds to an integrated luminosity of $6\,\text{fb}^{-1}$ of proton-proton (pp) collisions recorded at a centre-of-mass energy of 13 TeV. The analysis focuses on the region dominated by the $\overline{K}^*(892)^0$ resonance, which is denoted as $\overline{K}^{*0}$ for simplicity hereafter. The decay rate is analysed as a function of three angles in the helicity basis ($\cos\theta_K$, $\cos\theta_\mu$, ϕ_h), which describe the orientation of the decay products in their respective rest frames. This analysis follows the approach detailed in ref. [17] to determine the polarisation components, associated phase differences, and direct *CP* asymmetries for both the P-wave ($\overline{K}^{*0}$ vector meson) and S-wave (spin-zero) components of the $K^-\pi^+$ system. The branching fraction relative to the $B^0 \to J/\psi K^{*0}$ decay is also measured, providing updated inputs to constrain penguin contributions in $b \to c\bar{c}s$ transitions. Compared to the previous LHCb result [17], the precision of this analysis can achieve benefits not only from a nearly twofold increase in the integrated luminosity, but also from an increased $b\bar{b}$ production cross-section at the higher centre-of-mass energy, and from an optimised event selection that improves the sample purity. The larger data and simulation samples also allow for a significant reduction of the dominant systematic uncertainties, many of which were statistically limited in the previous measurement.

[1] The inclusion of charge-conjugate processes is implied throughout, unless otherwise noted.

JHEP10(2025)173

The remainder of this paper is organised as follows: a brief description of the LHCb detector and the simulation samples used is provided in section 2, the reconstruction of candidate decays and the event selection criteria are detailed in section 3, followed by the procedure for the fit to the mass distribution in section 4. The methodology for the angular analysis is summarised in section 5, and the determination of the branching fraction is explained in section 6. The results obtained from the Run 2 data, along with their associated uncertainties, are presented in section 7. These are then combined with previous LHCb measurements from Run 1 in section 8. Finally, section 9 provides the conclusions of this work.

2 The LHCb detector and simulation

The LHCb detector [19, 20] is a single-arm forward spectrometer covering the pseudorapidity range $2 < \eta < 5$, designed for the study of particles containing b or c quarks. The detector includes a high-precision tracking system consisting of a silicon-strip vertex detector surrounding the pp interaction region [21], a large-area silicon-strip detector located upstream of a dipole magnet with a bending power of about 4 T m, and three stations of silicon-strip detectors and straw drift tubes [22] placed downstream of the magnet. The tracking system provides a measurement of the momentum, p, of charged particles with a relative uncertainty that varies from 0.5% at low momentum to 1.0% at 200 GeV/c. The minimum distance of a track to a primary pp collision vertex (PV), the impact parameter (IP), is measured with a resolution of $(15 + 29/p_{\mathrm{T}})$ µm, where p_{T} is the component of the momentum transverse to the beam, in GeV/c. Different types of charged hadrons are distinguished using information from two ring-imaging Cherenkov detectors (RICH) [23]. Photons, electrons and hadrons are identified by a calorimeter system consisting of scintillating-pad and preshower detectors, an electromagnetic and hadronic calorimeter. Muons are identified by a system composed of alternating layers of iron and multiwire proportional chambers [24].

Simulation samples are generated to model the signal ($B_s^0 \to J/\psi \overline{K}^{*0}$) and normalisation ($B^0 \to J/\psi K^{*0}$) channels, as well as potential background contributions. Proton-proton collisions are generated using Pythia 8 [25] with a specific LHCb configuration [26]. Decays of hadronic particles are described by EvtGen [27], in which final-state radiation is generated using Photos [28]. The interaction of the generated particles with the detector and its response are implemented using the Geant4 toolkit [29] as described in ref. [30]. In the signal and normalisation channel simulations, the P-wave components were generated to match the angular distributions observed in the LHCb Run 1 analysis [17].

Several corrections to the simulated samples are applied to improve the agreement with data. Differences in the B_s^0/B^0 production kinematics and detector occupancy are corrected using a multivariate boosted decision tree (BDT) weighting technique [31]. These corrections are derived from the high-statistics $B^0 \to J/\psi K^{*0}$ control channel using simulation and background-subtracted data, and then applied to both B^0 and B_s^0 simulated samples. Corrections for particle identification (PID) efficiencies are applied using calibration samples and a kernel density estimation method, accounting for track kinematics and detector occupancy [32, 33]. Further corrections related to angular acceptance are discussed in section 5.2.

JHEP10(2025)173

3 Reconstruction and selection

Candidate $B_s^0 \to J/\psi \overline{K}^{*0}$ decays are reconstructed using pp collision data collected by the LHCb detector during Run 2. The online event selection employs a trigger system [34] consisting of a hardware stage followed by two software stages. The hardware trigger selects events based on high-p_{T} muons or high transverse energy calorimeter deposits; events passing any hardware decision are retained for this analysis. The first stage of the software trigger performs partial event reconstruction, selecting candidates primarily through signatures requiring displaced single muons, dimuons, or two-track vertices identified by multivariate algorithms [35]. The second software stage performs a full event reconstruction, selecting $J/\psi \to \mu^+\mu^-$ candidates with good vertex-fit quality, significant displacement from any PV, and a dimuon mass within $\pm 120\,\mathrm{MeV}/c^2$ of the known J/ψ mass [36].

The offline selection criteria are optimised for the Run 2 dataset, following a strategy similar to that used in the Run 1 analysis [17]. The J/ψ candidates are formed from two oppositely charged tracks identified as muons using information from the muon chambers and RICH detectors. The two tracks must have a small distance of closest approach (DOCA) between their trajectories and form a vertex with good vertex-fit quality. The dimuon mass is required to be within the range $[-48.0, +42.9]\,\mathrm{MeV}/c^2$ around the known J/ψ mass [36]. The $\overline{K}^{*0}$ candidates are formed from two oppositely charged tracks identified as a kaon and a pion using RICH information. Similar requirements as for the muons are applied to DOCA and vertex-fit quality. The mass of the $K^-\pi^+$ pair must be within $\pm 70\,\mathrm{MeV}/c^2$ of the known $\overline{K}^{*0}$ mass [36]. The B_s^0 candidates are formed by combining a J/ψ and a $\overline{K}^{*0}$ candidate, requiring them to originate from a common vertex with a good vertex-fit quality.

All four final-state tracks must be inconsistent with originating from any PV. The B_s^0 decay vertex must be significantly displaced from its associated PV, defined as that which gives the smallest χ^2_{IP} for the B_s^0 candidate. Here, χ^2_{IP} is defined as the difference in the vertex-fit χ^2 of a given PV reconstructed with and without the particle under consideration. The cosine of the angle between the B_s^0 momentum vector and the vector pointing from the associated PV to the B_s^0 decay vertex (direction angle, DIRA) is required to be greater than 0.999. To suppress candidates containing duplicate or partial track reconstructions, the minimum opening angle between any pair of final-state tracks is required to be greater than 0.5 mrad.

A kinematic fit [37] is performed to improve the resolution of the decay kinematics and the helicity angles. The fit constrains the dimuon mass to the known J/ψ mass and requires the B_s^0 candidate to originate from its associated PV.

3.1 Combinatorial background

A BDT classifier [38] with gradient boosting is used to suppress the large combinatorial background remaining after the initial selection. To account for variations in data-taking conditions, separate BDTs are trained for three distinct periods: 2015–2016, 2017, and 2018. Simulated $B_s^0 \to J/\psi \overline{K}^{*0}$ events, corrected as described in section 2, serve as the signal proxy. Data candidates from the high-mass sideband, $m(J/\psi K^-\pi^+) \in [5440, 5650]\,\mathrm{MeV}/c^2$, serve as the background proxy. The k-folding technique ($k = 10$) [39] is used during training. Fourteen variables, selected for their ability to discriminate between signal and combinatorial background, are used as inputs to the BDT. These include:

JHEP10(2025)173

- Track variables: minimum track $\chi^2_{\rm IP}$ with respect to any PV, maximum DOCA between final-state tracks, maximum track fit χ^2/ndf (chi-squared per degree of freedom) for hadron and muon tracks separately;
- Vertex variables: vertex-fit χ^2/ndf of the J/ψ and B^0_s decay vertices;
- Particle identification: variables quantifying the confidence of muon identification, and neural network probabilities indicating whether hadron tracks correspond to kaons or pions;
- Kinematics: transverse momentum of the B^0_s candidate;
- Flight information: B^0_s candidate proper decay time, B^0_s $\chi^2_{\rm IP}$ relative to its associated PV, B^0_s DIRA;
- Fit quality: χ^2 from the B^0_s kinematic fit.

The trained classifiers are applied to the respective data and simulation samples, and a selection requirement is applied to the BDT output for each data-taking period. This requirement is chosen to maximise the statistical precision of the angular analysis (section 5), which involves balancing the retention of signal events against the rejection of background. This selection retains approximately 92.7% of the signal candidates passing the preceding requirements, while rejecting around 95.6% of the combinatorial background. Multiple candidates from the same pp bunch crossing are rare ($\sim 0.05\%$) after this selection; all such candidates are retained [40].

3.2 Peaking background

Specific background sources involving misidentified particles or partially reconstructed decays can form peaking structures in the $m(J/\psi K^-\pi^+)$ spectrum, potentially biasing both the signal yield and angular distributions. These contributions are evaluated and suppressed. The backgrounds considered include $B^+ \to J/\psi K^+$, $B^0 \to J/\psi\pi^+\pi^-$, $B^0_s \to J/\psi\pi^+\pi^-$, $B^0_s \to J/\psi K^+K^-$, $\Lambda^0_b \to J/\psi pK^-$, and $\Lambda^0_b \to J/\psi p\pi^-$ decays. These backgrounds are studied using simulated samples, and their expected yields are evaluated taking into account the sample luminosity, selection efficiencies, production cross-section from ref. [41], fragmentation fractions from ref. [42], and decay branching fractions from ref. [36].

Dedicated vetoes based on alternative mass hypotheses are applied to suppress the dominant background contributions. These include $B^+ \to J/\psi K^+$ decays where the J/ψ and K^+ are combined with an unrelated pion, and decays such as $\Lambda^0_b \to J/\psi pK^-$ and $\Lambda^0_b \to J/\psi p\pi^-$ involving particle misidentification. A combination of mass and PID requirements is used to reduce contributions from $B^0 \to J/\psi\pi^+\pi^-$ and $B^0_s \to J/\psi\pi^+\pi^-$ decays.

After these steps, following the Run 1 analysis approach [17], the remaining small contributions (at the level of 1% of the signal yield) from $B^0 \to J/\psi\pi^+\pi^-$ [43], $B^0_s \to J/\psi K^+K^-$ [44], and $\Lambda^0_b \to J/\psi pK^-$ [45] decays are statistically subtracted. This is achieved by adding simulated decays for these channels to the data sample, using negative weights. These simulated events are added prior to the mass fit (section 4), weighted according to their known amplitude models and scaled to their estimated residual yields. The remaining background contributions are sufficiently small and therefore neglected.

JHEP10(2025)173

3.3 Candidates with degraded momentum

Decays in which final-state hadrons decay in flight or interact with detector material can lead to poorly measured momenta and contribute to tails in the reconstructed $m(J/\psi K^-\pi^+)$ distribution. This effect is particularly relevant for the B^0 control channel, where the tail extends significantly into the B_s^0 signal region. Approximately 3% of reconstructed B^0 candidates have masses above $5325\,\text{MeV}/c^2$, contaminating the B_s^0 peak. To suppress these contributions, a dedicated BDT classifier is trained using simulated $B^0 \to J/\psi K^{*0}$ events. Signal proxy events are those where both kaon and pion tracks reach at least the second tracking station downstream of the magnet without significant interaction or decay. Background proxy events are those where at least one hadron fails this condition. Nine input variables are used related to track-fit quality, consistency between tracking subsystems, ghost probability [46], the probability of being misidentified as muons, and track momenta. After applying simulation corrections and k-folding ($k = 10$), a loose requirement on the BDT output is applied to data and simulation. This selection significantly reduces the tail from poorly reconstructed B^0 decays. Specifically, the ratio of B^0 candidates falling within the B_s^0 mass window (defined as $\pm 30\,\text{MeV}/c^2$ around the known B_s^0 mass [36]) to the number of B_s^0 signal candidates in the same window is decreased from approximately 12.8% to 7.6%. This reduction is achieved while maintaining a high signal efficiency of approximately 97.8% for the B_s^0 decays.

4 Fit to the mass distribution

The sample of selected $J/\psi K^-\pi^+$ candidates, after the application of selection requirements (section 3) and the statistical subtraction of known peaking backgrounds (section 3.2), consists primarily of signal $B_s^0 \to J/\psi \overline{K}^{*0}$ decays, control channel $B^0 \to J/\psi K^{*0}$ decays, and combinatorial background. To determine the yields of the signal and control channels, as well as combinatorial background, an extended unbinned maximum-likelihood fit is performed to the $m(J/\psi K^-\pi^+)$ mass distribution. From the results of this fit, *sPlot* weights [47] are calculated, using $m(J/\psi K^-\pi^+)$ as the discriminating variable. These weights are then used to statistically separate the different signal and background components, providing the necessary background-subtracted distributions for the subsequent angular analysis (section 5).

To account for variations across data-taking periods and the dependence of the signal shape on the $K^-\pi^+$ mass ($m_{K\pi}$), the data sample is divided into twelve subsamples. These are based on three data-taking periods (2015–2016, 2017, 2018) and four bins in $m_{K\pi}$, each $35\,\text{MeV}/c^2$ wide and spanning the region centred around the known $\overline{K}^{*0}$ mass [36]. The fit is performed simultaneously across these subsamples.

The probability density function (PDF) used in the fit describes three main components: B^0 and B_s^0 signals, and combinatorial background. The B^0 and B_s^0 signal shapes are modelled using a customised double-sided Crystal Ball function (2DSCB). This function offers a description of the signal tails comparable to that of the Hypatia function used in the Run 1 analysis [17], particularly accounting for effects such as final-state radiation from muons (bremsstrahlung), while providing improved robustness in the fit minimisation process. The 2DSCB function is constructed as a sum of two DSCB components [48], sharing the

JHEP10(2025)173

same peak position μ and tail parameters $(\alpha_L, \alpha_R, n_L, n_R)$, but with different resolution parameters (σ_1, σ_2) combined with a relative fraction f_1,

$$\begin{aligned}\mathcal{P}_{\text{2DSCB}}(m;\vec{\vartheta}) =& f_1 \mathcal{P}_{\text{DSCB}}(m;\alpha_L,\alpha_R,n_L,n_R,\sigma_1,\mu) \\ &+ (1-f_1)\mathcal{P}_{\text{DSCB}}(m;\alpha_L,\alpha_R,n_L,n_R,\sigma_2,\mu),\end{aligned} \tag{4.1}$$

where $\vec{\vartheta}$ represents the set of shape parameters. For both B^0 and B_s^0 signals, the tail parameters and the fraction f_1 are shared within each $m_{K\pi}$ bin and are fixed to values determined from fits to simulation. The position of the B_s^0 peak, $\mu_{B_s^0}$, is constrained relative to the B^0 peak (μ_{B^0}) using the world-average mass difference Δm [36], i.e. $\mu_{B_s^0} = \mu_{B^0} + \Delta m$. The core Gaussian resolutions for the 2DSCB function are determined from fits to simulated B^0 events and shared between B^0 and B_s^0 decays. To account for potential differences between data and simulation, these simulation-based resolutions are adjusted in the fit to data using multiplicative scale factors, $s_{B_s^0}$ and s_{B^0}, applied independently to the signal and normalisation channels, respectively. These scale factors ($s_{B_s^0}$ and s_{B^0}) and the B^0 peak position (μ_{B^0}) are allowed to vary freely in the fit, determined independently for each $m_{K\pi}$ bin but shared across the data-taking years. Finally, the combinatorial background component is described by an exponential function, $\mathcal{P}_{\text{comb}}(m) \propto e^{k_{\text{comb}} m}$, where the slope parameter k_{comb} is allowed to vary freely in the fit for each subsample.

The full PDF per subsample is given by

$$\begin{aligned}\mathcal{P}_{\text{full}}(m;\vec{\vartheta},\mu_{B^0},\Delta m, s_{B^0}, s_{B_s^0}) =& N_{B_s^0}\mathcal{P}_{\text{2DSCB}}(m;\vec{\vartheta},\mu_{B^0}+\Delta m, s_{B_s^0}) \\ &+ N_{B^0}\mathcal{P}_{\text{2DSCB}}(m;\vec{\vartheta},\mu_{B^0}, s_{B^0}) \\ &+ N_{\text{comb}}\mathcal{P}_{\text{comb}}(m;k_{\text{comb}}),\end{aligned} \tag{4.2}$$

where $\vec{\vartheta}$ denotes the shape parameters that are fixed to values determined from simulation, while the yields $N_{B_s^0}$, N_{B^0}, and N_{comb} are free parameters in each subsample.

The simultaneous fit is performed across all twelve subsamples in the mass range $5150 < m(J/\psi K^-\pi^+) < 5650\,\text{MeV}/c^2$. Projections of the fit result, summed over all subsamples, are shown in figure 1. The overall yields, summed across all $m_{K\pi}$ bins and years, are determined to be

$$\begin{aligned}N_{B^0} &= 726\,540 \pm 860\,(\text{stat}) \pm 260\,(\text{syst}), \\ N_{B_s^0} &= \quad 6\,098 \pm \ 84\,(\text{stat}) \pm \ 39\,(\text{syst}),\end{aligned}$$

where the systematic uncertainties arise primarily from the choice of fit model (section 7). The ratio of these fitted yields, which is a key ingredient in the branching fraction measurement (section 6), is found to be

$$\frac{N_{B_s^0}}{N_{B^0}} = (8.39 \pm 0.12\,(\text{stat}) \pm 0.05\,(\text{syst})) \times 10^{-3},$$

where the small correlations between B^0 and B_s^0 yields are taken into account.

Based on the fit results within each subsample, *sPlot* weights [47] are calculated to statistically separate the signal, normalisation, and background components for the angular

JHEP10(2025)173

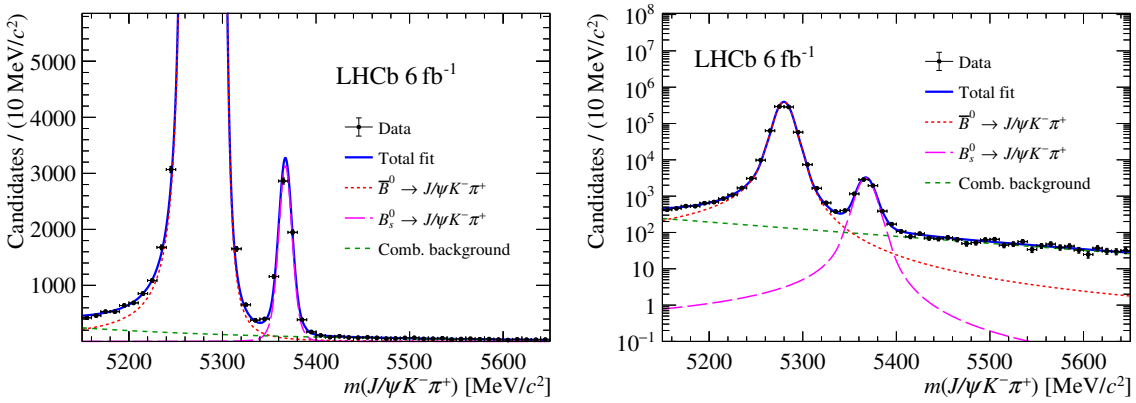

Figure 1. Projection of the simultaneous fit to the $m(J/\psi K^-\pi^+)$ distribution for the full Run 2 data sample, summed over data-taking periods and $m_{K\pi}$ bins. The distribution is shown with a (left) linear y-axis scale, where the vertical range is adjusted to highlight the B_s^0 signal, and a (right) logarithmic y-axis scale to display the full range. The data points and the total fit function, along with its components, are described in the legend.

analysis. A key assumption for the unbiased application of the *sPlot* technique is the lack of significant correlation between the discriminating variable ($m(J/\psi K^-\pi^+)$) and the variables of interest for the subsequent analysis (the angles: $\cos\theta_K$, $\cos\theta_\mu$, ϕ_h). This lack of correlation has been verified using the Kendall rank correlation test [49, 50] on simulation and data sidebands (p-values > 0.1). Residual correlations are accounted for using input from simulation, and considered when evaluating systematic uncertainties (section 7).

5 Angular analysis

The polarisation fractions, phase differences, and direct *CP* asymmetries of the $B_s^0 \to J/\psi \overline{K}^{*0}$ decay are extracted via an unbinned maximum-likelihood fit to the three helicity angles $\Omega_{\rm hel} = (\cos\theta_K, \cos\theta_\mu, \phi_h)$. The fit is performed on the background-subtracted data sample, obtained using the *sPlot* weights derived from the mass fit [51]. The analysis closely follows the methodology detailed in the previous LHCb measurement using Run 1 data [17].

5.1 Angular formalism

The decay is described in the helicity basis, where the helicity angles are defined as in ref. [17]. The analysis considers contributions from the spin-one (P-wave) $\overline{K}^{*0}$ resonance and an effective spin-zero (S-wave) $K\pi$ component. The time-integrated decay rate can be expressed in the helicity basis as [52]

$$\frac{\mathrm{d}\Gamma(\Omega_{\rm hel})}{\mathrm{d}\Omega_{\rm hel}} \propto \sum_{\alpha_\mu=\pm1} \left| \sum_{\lambda,J}^{|\lambda|\leq J} \sqrt{\frac{2J+1}{4\pi}} \mathcal{H}_\lambda^J e^{-i\lambda\phi_h} d^1_{\lambda,\alpha_\mu}(\theta_\mu) d^J_{-\lambda,0}(\theta_K) \right|^2 , \tag{5.1}$$

where $\lambda = 0, \pm1$ is the J/ψ helicity, $\alpha_\mu = \pm1$ is the difference between the helicities of the two muons, J is the spin of the $K\pi$ system ($J = 0$ for S-wave, $J = 1$ for P-wave), $\mathcal{H}_\lambda^J$ are the helicity amplitudes, and $d^j_{m'm}$ are the Wigner small d-matrices.

JHEP10(2025)173

Working in the transversity basis, the amplitudes $(A_0, A_\parallel, A_\perp, A_S)$ have definite *CP* properties, related to the helicity amplitudes via

$$\begin{aligned} A_0 &= \mathcal{H}^1_0, \\ A_\parallel &= \frac{1}{\sqrt{2}}(\mathcal{H}^1_{+1} + \mathcal{H}^1_{-1}), \\ A_\perp &= \frac{1}{\sqrt{2}}(\mathcal{H}^1_{+1} - \mathcal{H}^1_{-1}), \\ A_S &= \mathcal{H}^0_0. \end{aligned} \tag{5.2}$$

These transversity amplitudes are complex numbers, $A_k = |A_k|e^{i\delta_k}$ (for $k = 0, \parallel, \perp, S$), where $|A_k|$ is the magnitude and δ_k is the corresponding phase. For the *CP*-conjugate decay $\overline{B}^0_s \to (J/\psi \to \mu^+\mu^-)(K^{*0} \to K^+\pi^-)$, the corresponding amplitudes are denoted $\overline{A}_k$.

The differential decay rate can be expanded as a sum of ten terms involving products (a_k) of these amplitudes multiplied by specific angular functions $G_k(\Omega_{\rm hel})$,

$$\frac{\mathrm{d}\Gamma(\Omega_{\rm hel})}{\mathrm{d}\Omega_{\rm hel}} = \sum_{k=1}^{10} a_k G_k(\Omega_{\rm hel}). \tag{5.3}$$

The terms a_k involve bilinear products of the transversity amplitudes. Specifically, the terms with index $k = 1, 2, 3, 7$ correspond to the squared magnitudes $|A_0|^2, |A_\parallel|^2, |A_\perp|^2, |A_S|^2$, respectively. The remaining terms ($k = 4, 5, 6, 8, 9, 10$) represent interference between different transversity amplitudes. The explicit forms of a_k and G_k are given in table 1. For the terms representing squared amplitudes, the table also shows the correspondence between the summation index k and the respective polarisation state labels $(0, \parallel, \perp, S)$. This expansion is equivalent to that in ref. [52]. A similar expansion exists for the $\overline{B}^0_s$ decay rate using the amplitudes $\overline{A}_k$.

The direct *CP* asymmetry for a specific final-state polarisation k is defined using the partial decay rates $\Gamma_k = \int a_k G_k(\Omega_{\rm hel})\mathrm{d}\Omega_{\rm hel}$ integrated over angles (where a_k involves only $|A_k|^2$ or $|\overline{A}_k|^2$ for $k = 0, \parallel, \perp, S$),

$$A^{CP}_k = \frac{\overline{\Gamma}_k - \Gamma_k}{\overline{\Gamma}_k + \Gamma_k} \quad (k = 0, \parallel, \perp, S). \tag{5.4}$$

The analysis employs a simultaneous maximum-likelihood fit across the eight categories defined by the four $m_{K\pi}$ bins (section 4) and the two meson states (B^0_s and $\overline{B}^0_s$), tagged by the reconstructed kaon charge. This fit determines the physics asymmetries A^{CP}_k defined in eq. (5.4), along with parameters describing the *CP*-averaged decay dynamics. Introducing the *CP*-averaged partial decay rate for polarisation state k as $\Gamma^{\rm avg}_k = (\Gamma_k + \overline{\Gamma}_k)/2$, the *CP*-averaged parameters extracted by the fit are:

- The P-wave polarisation fractions f_k ($k = 0, \parallel, \perp$). These represent the fraction of the total *CP*-averaged P-wave decay rate ($\Gamma^{\rm avg}_{\rm P} = \Gamma^{\rm avg}_0 + \Gamma^{\rm avg}_\parallel + \Gamma^{\rm avg}_\perp$) associated with each polarisation state,

$$f_k = \frac{\Gamma^{\rm avg}_k}{\Gamma^{\rm avg}_{\rm P}} = \frac{\Gamma^{\rm avg}_k}{\Gamma^{\rm avg}_0 + \Gamma^{\rm avg}_\parallel + \Gamma^{\rm avg}_\perp}. \tag{5.5}$$

  By definition, these fractions satisfy the constraint $f_0 + f_\parallel + f_\perp = 1$.

JHEP10(2025)173

Index k	Amplitude product a_k	Angular function $G_k(\Omega_{\rm hel})$
1 (0)	$\lvert A_0\rvert^2$	$\frac{9}{16\pi}\cos^2\theta_K(1-\cos^2\theta_\mu)$
2 ($\parallel$)	$\lvert A_\parallel\rvert^2$	$\frac{9}{32\pi}(1-\cos^2\theta_K)(1-(1-\cos^2\theta_\mu)\cos^2\phi_h)$
3 ($\perp$)	$\lvert A_\perp\rvert^2$	$\frac{9}{32\pi}(1-\cos^2\theta_K)((1-\cos^2\theta_\mu)\cos^2\phi_h+\cos^2\theta_\mu)$
4	$\mathcal{I}m(A_\parallel^* A_\perp)$	$\frac{9}{16\pi}(1-\cos^2\theta_K)(1-\cos^2\theta_\mu)\sin(2\phi_h)$
5	$\mathcal{R}e(A_0^* A_\parallel)$	$\frac{9\sqrt{2}}{16\pi}\cos\theta_K\cos\theta_\mu\sqrt{(1-\cos^2\theta_K)(1-\cos^2\theta_\mu)}\cos\phi_h$
6	$\mathcal{I}m(A_0^* A_\perp)$	$\frac{9\sqrt{2}}{16\pi}\cos\theta_K\cos\theta_\mu\sqrt{(1-\cos^2\theta_K)(1-\cos^2\theta_\mu)}\sin\phi_h$
7 (S)	$\lvert A_S\rvert^2$	$\frac{3}{16\pi}(1-\cos^2\theta_\mu)$
8	$\mathcal{R}e(A_S^* A_\parallel)$	$\frac{3\sqrt{6}}{16\pi}\cos\theta_\mu\sqrt{(1-\cos^2\theta_K)(1-\cos^2\theta_\mu)}\cos\phi_h$
9	$\mathcal{I}m(A_S^* A_\perp)$	$\frac{3\sqrt{6}}{16\pi}\cos\theta_\mu\sqrt{(1-\cos^2\theta_K)(1-\cos^2\theta_\mu)}\sin\phi_h$
10	$\mathcal{R}e(A_S^* A_0)$	$\frac{3\sqrt{3}}{8\pi}\cos\theta_K(1-\cos^2\theta_\mu)$

Table 1. Angular basis functions $G_k(\Omega_{\rm hel})$ and the corresponding amplitude products a_k appearing in the differential decay rate eq. (5.3), as defined in ref. [52]. Also shown in parentheses in the first column are the corresponding transversity basis labels for the squared-amplitude terms.

- The S-wave fraction F_S. This represents the fraction of the total CP-averaged decay rate ($\Gamma^{\rm avg}_{\rm tot} = \Gamma^{\rm avg}_{\rm P} + \Gamma^{\rm avg}_S$) originating from the S-wave component,

$$F_S = \frac{\Gamma^{\rm avg}_S}{\Gamma^{\rm avg}_{\rm tot}} = \frac{\Gamma^{\rm avg}_S}{\Gamma^{\rm avg}_0 + \Gamma^{\rm avg}_\parallel + \Gamma^{\rm avg}_\perp + \Gamma^{\rm avg}_S}. \tag{5.6}$$

- The phase differences $\delta_\parallel - \delta_0$, $\delta_\perp - \delta_0$, and $\delta_S - \delta_0$, adopting the convention $\delta_0 = 0$.

The detailed parameterisation implemented in the likelihood function to extract these quantities is discussed further in section 5.3.

Within the simultaneous fit, the P-wave parameters ($f_0, f_\parallel, \delta_\parallel, \delta_\perp, A_0^{CP}, A_\parallel^{CP}, A_\perp^{CP}$) and the S-wave CP asymmetry (A_S^{CP}) are constrained to be the same across all $m_{K\pi}$ bins. The remaining S-wave parameters, the fraction F_S and the phase δ_S, are allowed to vary independently in each bin. The mass dependence of the interference between the S-wave and P-wave components is accounted for by scaling the interference terms ($k = 8, 9, 10$ in eq. (5.3)) by the complex factor $C_{\rm SP}e^{-i\Theta_{\rm SP}}$, which depends on the $K\pi$ mass spectrum. The same numerical values for $C_{\rm SP}$ are used as in ref. [17], and the interference phase $\Theta_{\rm SP}$ is absorbed into the definition of the fitted S-wave phase δ_S.

5.2 Angular acceptance

The detector geometry and selection criteria distort the observed angular distributions relative to the true decay rate described by eq. (5.3). This acceptance effect, represented by the function $\varepsilon(\Omega_{\rm hel})$, must be accounted for in the fit. The acceptance function is determined

JHEP10(2025)173

Index k	Amplitude product a_k	Normalised weight ξ_k/ξ_1
1	$\lvert A_0\rvert^2$	1
2	$\lvert A_\parallel\rvert^2$	1.4249 ± 0.0073
3	$\lvert A_\perp\rvert^2$	1.4489 ± 0.0074
4	$\lvert A_\parallel\rvert\lvert A_\perp\rvert \sin(\delta_\parallel - \delta_\perp)$	-0.0013 ± 0.0043
5	$\lvert A_0\rvert\lvert A_\parallel\rvert \cos(\delta_\parallel)$	-0.0189 ± 0.0029
6	$\lvert A_0\rvert\lvert A_\perp\rvert \sin(\delta_\perp)$	0.0027 ± 0.0028
7	$\lvert A_S\rvert^2$	1.2485 ± 0.0062
8	$\lvert A_S\rvert\lvert A_\parallel\rvert \cos(\delta_S - \delta_\parallel)$	-0.0412 ± 0.0040
9	$\lvert A_S\rvert\lvert A_\perp\rvert \sin(\delta_S - \delta_\perp)$	0.0072 ± 0.0040
10	$\lvert A_S\rvert\lvert A_0\rvert \cos(\delta_S)$	-0.6919 ± 0.0096

Table 2. Example normalisation weights ξ_k determined for Run 2 B_s^0 candidates in the third $m_{K\pi}$ bin with a K^- meson, normalised such that $\xi_1 = 1$. The index k corresponds to the terms in table 1. Uncertainties are statistical only, arising from the limited size of the simulation sample.

using simulated samples. To ensure these samples accurately reflect Run 2 data conditions, several corrections are applied to account for potential imperfections in simulating the detector response and particle kinematics. These corrections involve both kinematic weighting and an iterative procedure designed to ensure that the angular distributions in the corrected simulation match those observed in data, following strategies similar to previous LHCb analyses [17, 53]. The kinematic variables corrected via weighting include the total and transverse momentum of the B_s^0 meson and the final-state kaon and pion tracks, and the $K\pi$ mass. In the baseline approach, corrections for the B_s^0 and final-state track kinematics are primarily derived using the B^0 control channel, while the $m_{K\pi}$ correction, which weights the simulated $m_{K\pi}$ distribution to match that from background-subtracted B_s^0 data, is derived using the B_s^0 signal sample.

The acceptance correction is incorporated into the likelihood fit using the method of normalisation weights [54, 55]. This method involves calculating the integrals

$$\xi_k = \int \varepsilon(\Omega_{\text{hel}}) G_k(\Omega_{\text{hel}}) \mathrm{d}\Omega_{\text{hel}} \tag{5.7}$$

for each angular function G_k (defined in table 1) using the corrected simulation samples. These weights ξ_k are calculated separately for each of the eight analysis subsamples (4 $m_{K\pi}$ bins $\times$ 2 kaon charges) and are used directly in the construction of the likelihood function, obviating the need for an explicit parameterisation of $\varepsilon(\Omega_{\text{hel}})$. An example set of the normalisation weights is shown in table 2. Statistical uncertainties arising from the finite size of the simulation samples used to calculate the ξ_k weights are evaluated using bootstrap replicas, following standard resampling techniques [56], and propagated as systematic uncertainties on the measured physics parameters.

5.3 *CP* asymmetries

The maximum-likelihood fit described in section 5.1 aims to determine the direct physics *CP* asymmetries A_k^{CP} (defined in eq. (5.4)), alongside the *CP*-averaged polarisation fractions

JHEP10(2025)173

(f_k, F_S) and phases (δ_k), which were introduced and defined in section 5.1. These are the fundamental physics parameters extracted from the data.

To achieve this, the likelihood function models the decay rates for B_s^0 and $\overline{B}_s^0$ candidates separately, using a parameterisation based on these physics parameters. The *CP*-averaged polarisation fractions f_k $(k = 0, \|, \perp)$ and F_S, as defined by their relation to the *CP*-averaged partial decay rates in section 5.1, correspond to the average contributions of each polarisation state. These correspond to squared average amplitudes, denoted $|A_k|^2_{\rm avg}$. Specifically, $|A_k|^2_{\rm avg}$ is equivalent to f_k for P-waves, and for the S-wave, $|A_S|^2_{\rm avg}$ is related to F_S via $F_S = |A_S|^2_{\rm avg}/(1 + |A_S|^2_{\rm avg})$.

The overall normalisation yields for the physics decays B_s^0 $(N(B_s^0 \to f))$ and $\overline{B}_s^0$ $(N(\overline{B}_s^0 \to \overline{f}))$ are parameterised in terms of an effective average total yield $N_{\rm avg}$ (also determined by the fit) and an effective physics *CP* asymmetry $\mathbb{A}^{CP}_{\rm phys} = \sum_k |A_k|^2_{\rm avg} A_k^{CP}/(1 + |A_S|^2_{\rm avg})$,

$$N(B_s^0 \to f) = N_{\rm avg}(1 - \mathbb{A}^{CP}_{\rm phys}), \quad N(\overline{B}_s^0 \to \overline{f}) = N_{\rm avg}(1 + \mathbb{A}^{CP}_{\rm phys}). \tag{5.8}$$

The squared amplitude magnitudes for the individual B_s^0 and $\overline{B}_s^0$ decays, $|A_k|^2$ and $|\overline{A}_k|^2$ respectively, which determine the angular shape via the terms a_k (table 1), are then constructed within the model using the *CP*-violation parameter A_k^{CP}, the average magnitudes $|A_k|^2_{\rm avg}$, and the effective asymmetry $\mathbb{A}^{CP}_{\rm phys}$ via the relations

$$|A_k|^2 = \frac{|A_k|^2_{\rm avg}(1 - A_k^{CP})}{1 - \mathbb{A}^{CP}_{\rm phys}}, \quad |\overline{A}_k|^2 = \frac{|A_k|^2_{\rm avg}(1 + A_k^{CP})}{1 + \mathbb{A}^{CP}_{\rm phys}}. \tag{5.9}$$

This parameterisation provides the model for the underlying physics decay rates and shapes based on the parameters $(A_k^{CP},\ f_k,\ F_S,\ \delta_k,\ N_{\rm avg})$ determined by the fit.

However, the experimentally observed yields $N(B_s^0)$ and $N(\overline{B}_s^0)$ are affected by nuisance asymmetries arising from particle production and detection. The raw asymmetry observed in the data is defined as

$$A^{\rm raw} = \frac{N(\overline{B}_s^0) - N(B_s^0)}{N(\overline{B}_s^0) + N(B_s^0)}. \tag{5.10}$$

This raw asymmetry differs from the effective physics asymmetry $\mathbb{A}^{CP}_{\rm phys}$ (derived from the fit parameters A_k^{CP} and $|A_k|^2_{\rm avg}$). To account for this difference, the likelihood function incorporates the known nuisance asymmetries as fixed inputs. To do this, when modelling the observed asymmetry between the B_s^0 and $\overline{B}_s^0$ samples, the likelihood function uses an effective asymmetry constructed from the physics fit parameters A_k^{CP} combined with the relevant nuisance terms: $\kappa_s A_{\rm P} + A_{\rm D}(K\pi) + A_{\rm PID}(K\pi)$. Here, $A_{\rm P}$ is the production asymmetry between $\overline{B}_s^0$ and B_s^0, $A_{\rm D}(K\pi)$ is the detection asymmetry between the $K^+\pi^-$ and $K^-\pi^+$ pairs in the final state, and $A_{\rm PID}(K\pi)$ is the corresponding asymmetry induced by the hadron PID selection requirements. The factor κ_s accounts for the dilution due to B-meson mixing, following the definition given in ref. [17]. This procedure allows the fit to determine the true physics asymmetries A_k^{CP}.

The production asymmetries $A_{\rm P}(B_s^0)$ and $A_{\rm P}(B^0)$ used in this analysis are taken from measurements performed at $\sqrt{s} = 8\,\text{TeV}$ [57]. For the B_s^0 analysis, while the $A_{\rm P}(B_s^0)$ value

JHEP10(2025)173

might slightly differ from the true asymmetry at $\sqrt{s} = 13\,\text{TeV}$, its impact on the determination of A_k^{CP} is negligible owing to the very small B_s^0 mixing dilution factor, κ_s, determined to be approximately 0.08% for this decay. The instrumental detection asymmetry $A_{\text{D}}(K\pi)$ and PID asymmetry $A_{\text{PID}}(K\pi)$ are evaluated for the Run 2 dataset using dedicated calibration samples in data [32, 33, 58]. The calculated asymmetries for the B_s^0 sample (relevant for the $K^-\pi^+$ final state) are

$$A_{\text{D}}^{B_s^0}(K\pi) = (+0.802 \pm 0.030\,(\text{stat}) \pm 0.011\,(\text{syst}))\%,$$
$$A_{\text{PID}}^{B_s^0}(K\pi) = (+0.45 \pm 0.22\,(\text{stat}) \pm 0.05\,(\text{syst}))\%.$$

These values are incorporated as fixed inputs into the likelihood fit to extract the physics asymmetries A_k^{CP}.

The B^0 control channel is analysed analogously. For this channel, the $A_{\text{P}}(B^0)$ value from the 8 TeV measurement, along with its respective detection and PID asymmetries evaluated for Run 2, are used. The dilution factor for the B^0 channel, κ_d, is significantly larger (approximately 40%); however, the potential discrepancy in $A_{\text{P}}(B^0)$ due to the different centre-of-mass energy is considered small when compared to the statistical precision of the control channel results and the uncertainty on the $A_{\text{P}}(B^0)$ measurement itself, and is thus deemed valid and used in this analysis. The results of the fit to the B^0 decay are checked for consistency with *CP* symmetry, validating the treatment of the instrumental effects.

6 Branching ratio measurement

The branching fraction of the $B_s^0 \to J/\psi \overline{K}^{*0}$ decay is measured relative to the topologically similar and CKM-favoured decay $B^0 \to J/\psi K^{*0}$, which acts as a normalisation channel. This relative measurement strategy, identical to that used in ref. [17], allows for the cancellation of several systematic uncertainties.

6.1 Measurement strategy

The ratio of branching fractions is given by

$$\frac{\mathcal{B}(B_s^0 \to J/\psi \overline{K}^{*0})}{\mathcal{B}(B^0 \to J/\psi K^{*0})} = \frac{N_{B_s^0 \to \overline{K}^{*0}}}{N_{B^0 \to K^{*0}}} \times \frac{\varepsilon_{B^0}}{\varepsilon_{B_s^0}} \times \frac{f_d}{f_s}, \tag{6.1}$$

where $N_{B_s^0 \to \overline{K}^{*0}}$ ($N_{B^0 \to K^{*0}}$) is the yield of signal (normalisation) decays originating purely from the P-wave $\overline{K}^{*0}(K^{*0})$ resonance, $\varepsilon_{B_s^0}$ (ε_{B^0}) is the corresponding total efficiency, and f_d/f_s is the ratio of fragmentation fractions [42].

The yields $N_{B_s^0(B^0)}$ obtained from the mass fit (section 4) include contributions from all partial waves. Similarly, the efficiencies $\varepsilon'_{B_s^0(B^0)}$ estimated from simulation are based on the generator-level angular distributions. Corrections are therefore required, following the method detailed in ref. [17]. A factor $F_{\text{decay}}^{\text{P}}$ corrects the fitted yield to obtain the P-wave yield ($N_{B\to X} = N_B \times F_{\text{decay}}^{\text{P}}$), and a factor c_{decay} corrects the simulation-based efficiency to account for the differences between the true angular distribution of the data and that used in the simulation. Thus, the overall efficiency is $\varepsilon = \varepsilon' \times c_{\text{decay}}$, where ε' accounts for detector

JHEP10(2025)173

acceptance and reconstruction efficiencies, and $c_{\rm decay}$ accounts for angular mismodelling. Combining these, the relative branching fraction becomes

$$\frac{\mathcal{B}(B_s^0 \to J/\psi \overline{K}^{*0})}{\mathcal{B}(B^0 \to J/\psi K^{*0})} = \frac{N_{B_s^0}}{N_{B^0}} \times \frac{\varepsilon'_{B^0}}{\varepsilon'_{B_s^0}} \times \frac{\zeta_{B^0}}{\zeta_{B_s^0}} \times \frac{f_d}{f_s}, \tag{6.2}$$

where the combined angular correction factor is $\zeta \equiv c_{\rm decay}/F^{\rm P}_{\rm decay}$. The explicit calculation of $F^{\rm P}_{\rm decay}$ and $c_{\rm decay}$ using results from the angular analysis is detailed below. The absolute branching fraction for $B_s^0 \to J/\psi \overline{K}^{*0}$ is subsequently obtained using the result from the Belle measurement [59] for $\mathcal{B}(B^0 \to J/\psi K^{*0})$, detailed in section 7.2.

6.2 Relative efficiencies from simulation

The ratio of total efficiencies, $\varepsilon'_{B^0}/\varepsilon'_{B_s^0}$, accounting for geometrical acceptance as well as trigger, reconstruction, and selection efficiencies, is determined using the corrected simulation samples described in section 2. It is determined separately for each data-taking period and then averaged, weighted by the measured signal yields per period. The average efficiency ratio obtained is

$$\frac{\varepsilon'_{B^0}}{\varepsilon'_{B_s^0}} = 0.943 \pm 0.006,$$

where the uncertainty is statistical only.

6.3 Corrections from angular analysis

The angular correction factors depend on the measured transversity amplitudes and acceptance weights ξ_k. Following the methodology described in ref. [17], the fraction of the fitted yield corresponding to the P-wave component is given by

$$F^{\rm P}_{\rm decay} = \frac{\sum_{k=1}^{6} \xi_k a_k}{\sum_{k=1}^{10} \xi_k a_k C_k}, \tag{6.3}$$

and the efficiency correction factor, accounting for differences between the angular distribution measured in data and that used in the simulation, is

$$c_{\rm decay} = \frac{\sum_{k=1}^{6} \xi_k a_k(\vec{A}_{\rm data})}{\sum_{k=1}^{6} \xi_k a_k(\vec{A}_{\rm sim})}. \tag{6.4}$$

In these expressions, a_k are the amplitude products (listed in table 1) evaluated using the measured amplitudes, and C_k incorporates the interference factors, with $C_k = 1$ for diagonal terms and $C_k = C_{\rm SP}$ for S-P interference. For the efficiency correction factor $c_{\rm decay}$, the numerator is evaluated using the amplitudes measured from data ($\vec{A}_{\rm data}$), while the denominator uses the amplitudes assumed in the simulation ($\vec{A}_{\rm sim}$). The acceptance weights ξ_k are determined once from the simulation sample and are the same in both the numerator and denominator.

These factors are calculated separately for the B_s^0 and B^0 channels using their respective angular fit results. The ratio of the combined factors required for eq. (6.2) is determined as

$$\frac{\zeta_{B^0}}{\zeta_{B_s^0}} = 1.015 \pm 0.034\,(\text{stat}) \pm 0.017\,(\text{syst}).$$

JHEP10(2025)173

The first uncertainty is statistical, propagated from the angular fit uncertainties, and the second is systematic, obtained by propagating the systematic variations of the angular parameters evaluated in section 7.1. With all components for the calculation of the relative branching fraction (eq. (6.2)) determined, the results are presented in section 7.2.

7 Results and uncertainties

This section presents the results of the angular analysis and the branching fraction measurement based on the Run 2 dataset. The determination of statistical and systematic uncertainties follows standard procedures, similar to those described in the Run 1 analysis [17], adapted for the specific conditions and models used here.

7.1 Angular and *CP*-violation parameters

The central values for the P-wave and S-wave parameters are determined from the simultaneous angular fit described in section 5. The main results for the P-wave parameters from the Run 2 dataset are presented below. Detailed results for the S-wave parameters, determined per $m_{K\pi}$ bin, and the full breakdown of systematic uncertainties for all parameters, are given in tables 3 and 4. Figure 2 shows the projection of the fit onto the background-subtracted data. The full correlation matrix for the fitted parameters is provided in appendix A.

7.1.1 Run 2 P-wave polarisation fractions and *CP* asymmetries

The P-wave polarisation fractions obtained from the Run 2 data, averaged over the $m_{K\pi}$ range, are

$$\begin{aligned} f_0 &= 0.534 \pm 0.012\,(\text{stat}) \pm 0.009\,(\text{syst}), \\ f_\parallel &= 0.211 \pm 0.014\,(\text{stat}) \pm 0.005\,(\text{syst}). \end{aligned}$$

The corresponding direct *CP* asymmetries for the P-wave components, also averaged over the $m_{K\pi}$ range, are measured to be

$$\begin{aligned} A_0^{CP} &= 0.014 \pm 0.029\,(\text{stat}) \pm 0.007\,(\text{syst}), \\ A_\parallel^{CP} &= -0.055 \pm 0.065\,(\text{stat}) \pm 0.007\,(\text{syst}), \\ A_\perp^{CP} &= 0.060 \pm 0.057\,(\text{stat}) \pm 0.016\,(\text{syst}). \end{aligned}$$

These *CP* asymmetries are consistent with zero. The phases $\delta_\parallel$ and $\delta_\perp$ are also determined and presented in table 3.

Statistical uncertainties are determined using a bootstrap method [56], where the entire analysis chain is repeated on multiple datasets resampled from the original data. Systematic uncertainties are obtained by considering variations in the analysis procedure, modelling assumptions, and external inputs. Individual systematic uncertainties are assumed to be uncorrelated, and the total systematic uncertainty is calculated as the quadratic sum of these contributions. The main sources considered are summarised below, grouped according to their origin. Detailed contributions for each parameter are listed in tables 3 and 4.

JHEP10(2025)173

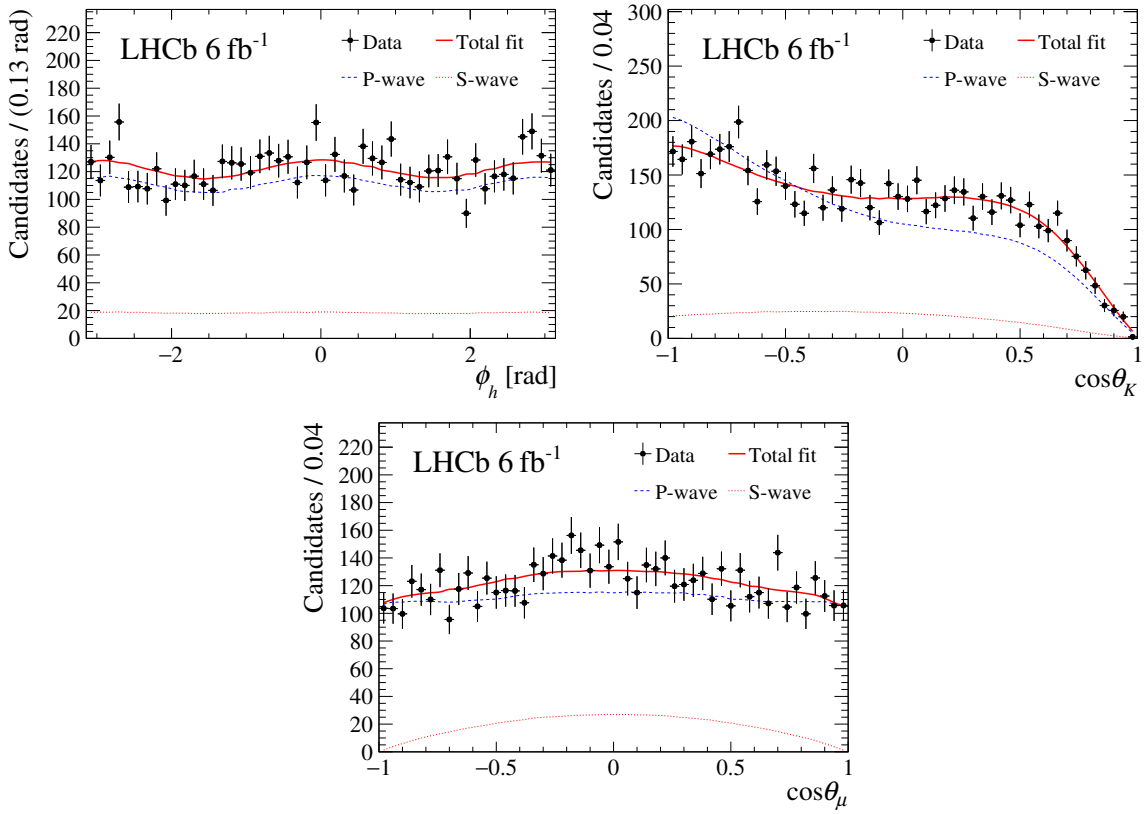

Figure 2. Projections of the angular fit result onto the helicity angles (top left) $\cos\theta_K$, (top right) $\cos\theta_\mu$, and (bottom) ϕ_h for the background-subtracted $B_s^0 \to J/\psi \overline{K}^*(892)^0$ data sample (black points with error bars), summed over all subsamples. The overall fit model (red solid line) is shown, along with its P-wave (blue dashed) and S-wave (orange dotted) components. Interference terms between S- and P-wave, which are part of the total fit model, are not explicitly shown but contribute to the overall shape; their effect can lead to regions where individual wave components appear to exceed the total fit projection.

7.1.2 Systematic uncertainties related to the mass fit

These uncertainties affect the calculation of the *sPlot* weights and consequently propagate to the angular analysis, influencing the measurement of angular parameters.

Mass fit model. Assessed by repeating the analysis using alternative PDF shapes (Hypatia function for signal peaks [60], Chebyshev polynomial for background) for the mass fit (section 4).

Peaking backgrounds. Determined by varying the yields of the statistically subtracted peaking backgrounds (section 3.2) within their uncertainties ($\pm 3\sigma$).

Exotic contributions. The potential impact of exotic state contributions, such as $T_{c\bar{c}1}(4200)^{\pm}$ and $T_{c\bar{c}1}(4430)^{\pm}$ produced in $B \to T_{c\bar{c}1} K$ ($T_{c\bar{c}1} \to J/\psi\pi$) decays [61], which yield the same final-state particles as the signal, is estimated using the B^0 control channel. An additional selection $\cos\theta_K > -0.6$ is applied to the B^0 sample, designed

JHEP10(2025)173

empirically to suppress such contributions. The systematic uncertainty assigned to the corresponding B_s^0 analysis results is taken as the maximum deviation observed in the B^0 parameters due to this selection.

Mass-angle correlations. Potential biases from residual correlations between $m(J/\psi K^-\pi^+)$ and helicity angles are primarily evaluated by performing the mass fit in five bins of $\cos\theta_\mu$. Correlations with the other helicity angles, $\cos\theta_K$ and ϕ_h, are found to be negligible, and their potential effects are neglected.

7.1.3 Systematic uncertainties related to the angular analysis

These uncertainties arise from the angular fitting procedure, the inputs to the fit, and the modelling of the angular distributions. They directly impact the determination of the polarisation fractions, phase differences, and *CP* asymmetries.

Simulation sample size Estimated by bootstrapping the simulation samples used to calculate the acceptance normalisation weights (ξ_k).

***C*$_{SP}$ factor.** Assessed by varying the $C_{\rm SP}$ values based on different lineshape models for the interfering S- and P-waves, following the procedure in ref. [17].

D-wave contribution. Estimated using pseudoexperiments generated with a small D-wave component (found to be $\sim 0.4\%$ on average from a fit to data) and fitted with the baseline model.

***CP* violation in δ_k phases.** Evaluated by allowing for potential differences between the δ_k phases for B_s^0 and $\overline{B}{}_s^0$ decays ($\Delta\delta_k \equiv \delta_k(B_s^0) - \delta_k(\overline{B}{}_s^0) \neq 0$) for the P-wave components in a variant fit.

Simulation corrections. Assessed by comparing results using the baseline simulation corrections (section 5.2, kinematic reweighting primarily from B^0 mesons) versus corrections derived directly using only B_s^0 samples.

Fit model bias. Checked using pseudoexperiments generated according to the baseline fit result and fitted with the same procedure.

External *CP* asymmetries. Uncertainties from the measured production and instrumental asymmetries ($A_{\rm P}, A_{\rm D}, A_{\rm PID}$) are propagated to the physics *CP* asymmetries A_k^{CP}.

7.2 Branching fraction

Substituting the ratio of fitted yields $N_{B_s^0}/N_{B^0}$ (section 4), the efficiency ratio $\varepsilon'_{B^0}/\varepsilon'_{B_s^0}$ (section 6.2), the angular correction ratio $\zeta_{B^0}/\zeta_{B_s^0}$ (section 6.3), and the hadronisation fraction ratio $f_d/f_s = 3.939 \pm 0.123$ [42] into eq. (6.2), the relative branching fraction for the Run 2 dataset is found to be

$$\frac{\mathcal{B}(B_s^0 \to J/\psi \overline{K}^{*0})}{\mathcal{B}(B^0 \to J/\psi K^{*0})} = (3.08 \pm 0.11\,(\text{stat}) \pm 0.06\,(\text{syst}) \pm 0.10\,(\frac{f_d}{f_s}))\%.$$

JHEP10(2025)173

Parameter	A_0^{CP}	$A_\parallel^{CP}$	$A_\perp^{CP}$	f_0	$f_\parallel$	$\delta_\parallel$	$\delta_\perp$
Measured value	0.014	−0.055	0.060	0.534	0.211	2.879	0.057
Statistical uncertainty	0.029	0.065	0.057	0.012	0.014	0.085	0.065
Mass fit model	0.001	—	—	0.001	—	—	0.001
Peaking bkg.	—	0.001	—	—	—	0.002	0.001
Exotics pollution	0.003	0.001	0.003	0.004	0.002	0.012	0.012
Mass–$\cos\theta_\mu$ correlation	0.002	—	0.004	0.002	0.001	0.005	0.002
Ang. Acc. (Sim. size)	0.001	0.004	0.004	0.001	0.001	0.005	0.004
$C_{\rm SP}$ factor	—	0.002	0.001	—	0.001	0.003	0.005
D-wave contribution	0.005	0.002	0.014	0.001	—	0.001	0.003
$\Delta\delta_k \neq 0$	—	—	—	—	—	0.004	0.003
Simulation corrections	—	0.004	—	0.008	0.004	0.009	0.010
Bias in model	0.001	0.001	—	0.001	0.001	0.001	0.001
External CP asym.	0.002	0.002	0.002	—	—	—	—
Quadratic sum of syst.	0.007	0.007	0.016	0.009	0.005	0.018	0.018
Total uncertainty	0.030	0.066	0.059	0.015	0.015	0.087	0.068

Table 3. Summary of results and uncertainties for P-wave parameters obtained in $B_s^0 \to J/\psi \overline{K}^{*0}$ decays, from the Run 2 data analysis. Central values and statistical uncertainties are from the baseline fit. Systematic uncertainties from different sources are listed, along with their quadratic sum. The total uncertainty is the quadratic sum of statistical and total systematic uncertainties. The phases are shown in radians. Values below 5×10^{-4} are indicated by "—".

The statistical uncertainty combines contributions from the yields and the ratio of the angular correction factors. The systematic uncertainty includes contributions from the fit model variations and the angular-correction ratio. The uncertainty labelled $\frac{f_d}{f_s}$ is due to the hadronisation fraction ratio. The dominant systematic uncertainties on the relative branching fraction originate from the choice of mass fit models (section 7.1.2) and the propagation of uncertainties from the angular analysis parameters (evaluated in section 7.1) via the correction factor ratio $\zeta_{B^0}/\zeta_{B_s^0}$ (defined in section 6.3). Other potential systematic uncertainties are found to largely cancel in the ratio.

The absolute branching fraction $\mathcal{B}(B_s^0 \to J/\psi \overline{K}^{*0})$ from the Run 2 dataset is obtained by multiplying the relative branching fraction measured above by an external value for the branching fraction of the normalisation channel, $\mathcal{B}(B^0 \to J/\psi K^{*0})$. For consistency with the amplitude analysis approach used here and in the previous LHCb measurement [17], which explicitly separates partial waves but without explicit consideration of exotic states such as $T_{c\bar{c}1}$ resonances, the result from the Belle collaboration [59] is used instead of the PDG average [36], $\mathcal{B}(B^0 \to J/\psi K^{*0})_{\rm Belle} = (1.29 \pm 0.05\,({\rm stat}) \pm 0.13\,({\rm syst})) \times 10^{-3}$. As this measurement was performed at the $\Upsilon(4S)$ resonance assuming equal production fractions $f^{00} = f^{+-} = 0.5$, a correction is needed because the measured production

JHEP10(2025)173

Parameter	A_S^{CP}	$m_{K\pi}^{\text{bin0}}$		$m_{K\pi}^{\text{bin1}}$		$m_{K\pi}^{\text{bin2}}$		$m_{K\pi}^{\text{bin3}}$	
		F_S	δ_S	F_S	δ_S	F_S	δ_S	F_S	δ_S
Measured value	0.081	0.420	−0.557	0.076	0.556	0.083	1.376	0.243	1.861
Statistical uncertainty	0.085	0.096	0.110	0.019	0.161	0.023	0.075	0.057	0.083
Mass fit model	0.002	0.001	0.005	—	0.003	0.001	0.004	0.001	0.002
Peaking bkg.	0.001	0.002	0.003	—	—	—	0.003	0.001	0.005
Exotics pollution	0.001	0.002	0.006	—	0.008	0.001	0.005	0.007	0.019
Mass–$\cos\theta_\mu$ correlation	0.015	0.042	0.037	0.001	0.003	0.006	0.003	0.008	0.004
Ang. Acc. (Sim. size)	0.007	0.008	0.008	0.001	0.012	0.002	0.005	0.004	0.006
C_{SP} factor	0.001	0.012	0.052	0.004	0.001	0.003	0.001	0.003	0.006
D-wave contribution	0.018	0.001	0.016	0.002	0.002	0.002	0.001	0.002	0.001
$\Delta\delta_k \neq 0$	0.001	0.002	0.001	—	0.002	—	—	0.003	0.002
Simulation corrections	—	0.051	0.011	0.002	0.003	0.002	0.009	0.018	0.060
Bias in model	0.002	0.003	0.017	0.003	0.006	0.001	0.003	0.001	0.003
External *CP* asym.	0.002	—	—	—	—	—	—	—	—
Quadratic sum of syst.	0.024	0.068	0.070	0.006	0.017	0.007	0.013	0.022	0.064
Total uncertainty	0.088	0.118	0.131	0.020	0.162	0.024	0.076	0.061	0.104

Table 4. Summary of results and uncertainties for S-wave parameters obtained in $B_s^0 \to J/\psi K^-\pi^+$ decays, from the Run 2 data analysis. Central values and statistical uncertainties are from the baseline fit. Systematic uncertainties from different sources are listed, along with their quadratic sum. The total uncertainty is the quadratic sum of statistical and total systematic uncertainties. The phases are shown in radians. Values below 5×10^{-4} are indicated by "—".

ratio $R^{+/0} \equiv f^{+-}/f^{00} = \Gamma(\Upsilon(4S) \to B^+B^-)/\Gamma(\Upsilon(4S) \to B^0\overline{B}^0) = 1.052 \pm 0.031$ [8] deviates from unity. The correction factor is calculated as $C = (1 + R^{+/0})/2 = 1.026 \pm 0.016$.

Using this correction factor, the absolute branching fraction for the signal decay from the Run 2 dataset is determined as

$$\begin{aligned}\mathcal{B}(B_s^0 \to J/\psi \overline{K}^{*0}) &= \frac{\mathcal{B}(B_s^0 \to J/\psi \overline{K}^{*0})}{\mathcal{B}(B^0 \to J/\psi K^{*0})} \times C \times \mathcal{B}(B^0 \to J/\psi K^{*0})_{\text{Belle}} \\ &= (4.07 \pm 0.15\,(\text{stat}) \pm 0.07\,(\text{syst}) \pm 0.13\,(\frac{f_d}{f_s}) \pm 0.45\,(\mathcal{B}_{B^0})) \times 10^{-5}.\end{aligned}$$

The uncertainties are ordered as: statistical, systematic, from f_d/f_s, and from other external inputs. This result is consistent with the previous LHCb measurement [17] and the current world average [36].

8 Combination with LHCb Run 1 results

The results obtained in this analysis (section 7) are consistent with the previous LHCb measurements using the Run 1 dataset [17]. A combination of the Run 1 and Run 2 results

JHEP10(2025)173

is performed using the Best Linear Unbiased Estimator (BLUE) method [62], taking into account correlations between uncertainties.

For the angular parameters, statistical uncertainties are treated as uncorrelated between the two datasets. Systematic uncertainties related to shared theoretical inputs or methodologies (e.g. $C_{\rm SP}$ factor modelling, external asymmetry evaluations) are considered 100% correlated, while dataset-specific uncertainties (e.g. simulation sample size, fit model choices specific to Run 1 or Run 2, background modelling) are treated as uncorrelated. The combined results for the P-wave polarisation fractions and *CP* asymmetries are

$$\begin{aligned} f_0 &= 0.528 \pm 0.011\,(\text{stat}) \pm 0.009\,(\text{syst}), \\ f_\parallel &= 0.205 \pm 0.012\,(\text{stat}) \pm 0.005\,(\text{syst}), \\ A_0^{CP} &= 0.021 \pm 0.026\,(\text{stat}) \pm 0.007\,(\text{syst}), \\ A_\parallel^{CP} &= -0.073 \pm 0.060\,(\text{stat}) \pm 0.007\,(\text{syst}), \\ A_\perp^{CP} &= 0.057 \pm 0.049\,(\text{stat}) \pm 0.014\,(\text{syst}). \end{aligned}$$

For the branching fraction combination, the relative measurement $\mathcal{B}(B_s^0 \to J/\psi \overline{K}^{*0})/\mathcal{B}(B^0 \to J/\psi K^{*0})$ from Run 1 [17] is updated before being used. It was originally reported as $(2.99 \pm 0.14\,(\text{stat}) \pm 0.12\,(\text{syst}) \pm 0.17\,(\frac{f_d}{f_s}))\%$, depended on an older determination of the hadronisation fraction ratio [63]. Since the measurement scales with f_d/f_s, this Run 1 result is recalculated using the latest value appropriate for Run 1 conditions, $f_s/f_d = 0.2387 \pm 0.0075$ [42]. This recalculation yields an updated Run 1 branching fraction ratio of $(3.24 \pm 0.15\,(\text{stat}) \pm 0.13\,(\text{syst}) \pm 0.11\,(\frac{f_d}{f_s}))\%$, which is used in the combination presented below.

The updated Run 1 value is combined with the Run 2 result from section 7.2 using the BLUE method. Statistical uncertainties are treated as uncorrelated. The systematic uncertainty arising from the external f_d/f_s ratio is treated as 100% correlated, while other systematic uncertainties specific to each analysis are assumed uncorrelated. The combined relative branching fraction is found to be

$$\frac{\mathcal{B}(B_s^0 \to J/\psi \overline{K}^{*0})}{\mathcal{B}(B^0 \to J/\psi K^{*0})} = (3.12 \pm 0.09\,(\text{stat}) \pm 0.06\,(\text{syst}) \pm 0.10\,(\frac{f_d}{f_s}))\%.$$

The combined absolute branching fraction is obtained by multiplying this ratio by the corrected Belle branching fraction for the normalisation channel (defined in section 7.2), and is determined as

$$\mathcal{B}(B_s^0 \to J/\psi \overline{K}^{*0}) = (4.13 \pm 0.12\,(\text{stat}) \pm 0.07\,(\text{syst}) \pm 0.14\,(\frac{f_d}{f_s}) \pm 0.45\,(\mathcal{B}_{B^0})) \times 10^{-5}.$$

9 Conclusions

This paper presents an angular analysis of the $B_s^0 \to J/\psi \overline{K}^*(892)^0$ decay, performed using pp collision data collected by the LHCb experiment at $\sqrt{s} = 13\,\text{TeV}$ during 2015–2018, corresponding to an integrated luminosity of $6\,\text{fb}^{-1}$. The P-wave polarisation fractions and direct *CP* asymmetries, presented in section 7.1.1, along with S-wave parameters and the branching fraction (section 7.2), significantly improve upon previous measurements. The measured *CP* asymmetries are consistent with zero within uncertainties.

JHEP10(2025)173

Combining these Run 2 results with those from Run 1 [17], as detailed in section 8, yields the most precise determinations to date of the angular parameters and the relative branching fraction $\mathcal{B}(B_s^0 \to J/\psi \overline{K}^*(892)^0)/\mathcal{B}(B^0 \to J/\psi K^*(892)^0))$. The combination also provides an updated value for the absolute branching fraction, determined using external input for the normalisation channel from the Belle collaboration [59]. These precise results provide crucial inputs for constraining penguin contributions to the *CP*-violating phase ϕ_s measured in $b \to c\bar{c}s$ decays. However, as established in the previous analysis of this channel [17], a quantitative constraint based solely on $B_s^0 \to J/\psi \overline{K}^{*0}$ decays remains limited by theoretical uncertainties in the hadronic form factors. The full benefit of the improved experimental precision will therefore only be realised in a future combined analysis that also incorporates results from SU(3)-partner decays, such as $B^0 \to J/\psi \rho^0$. Continued improvements in experimental precision with larger datasets at LHCb are anticipated to further refine these constraints and enhance the sensitivity to potential new physics in the B_s^0 meson system.

Acknowledgments

We express our gratitude to our colleagues in the CERN accelerator departments for the excellent performance of the LHC. We thank the technical and administrative staff at the LHCb institutes. We acknowledge support from CERN and from the national agencies: ARC (Australia); CAPES, CNPq, FAPERJ and FINEP (Brazil); MOST and NSFC (China); CNRS/IN2P3 (France); BMBF, DFG and MPG (Germany); INFN (Italy); NWO (Netherlands); MNiSW and NCN (Poland); MCID/IFA (Romania); MICIU and AEI (Spain); SNSF and SER (Switzerland); NASU (Ukraine); STFC (U.K.); DOE NP and NSF (U.S.A.). We acknowledge the computing resources that are provided by ARDC (Australia), CBPF (Brazil), CERN, IHEP and LZU (China), IN2P3 (France), KIT and DESY (Germany), INFN (Italy), SURF (Netherlands), Polish WLCG (Poland), IFIN-HH (Romania), PIC (Spain), CSCS (Switzerland), and GridPP (U.K.). We are indebted to the communities behind the multiple open-source software packages on which we depend. Individual groups or members have received support from Key Research Program of Frontier Sciences of CAS, CAS PIFI, CAS CCEPP, Fundamental Research Funds for the Central Universities, and Sci. & Tech. Program of Guangzhou (China); Minciencias (Colombia); EPLANET, Marie Skłodowska-Curie Actions, ERC and NextGenerationEU (European Union); A*MIDEX, ANR, IPhU and Labex P2IO, and Région Auvergne-Rhône-Alpes (France); Alexander-von-Humboldt Foundation (Germany); ICSC (Italy); Severo Ochoa and María de Maeztu Units of Excellence, GVA, XuntaGal, GENCAT, InTalent-Inditex and Prog. Atracción Talento CM (Spain); SRC (Sweden); the Leverhulme Trust, the Royal Society and UKRI (U.K.).

A Correlation matrix

The correlations between model parameters used in the angular analysis of B_s^0 signal decays are listed in table 5.

JHEP10(2025)173

	A_S^{CP}	A_0^{CP}	$A_\parallel^{CP}$	$A_\perp^{CP}$	$F_S^{826-861}$	$F_S^{861-896}$	$F_S^{896-931}$	$F_S^{931-966}$	$\delta_S^{826-861}$	$\delta_S^{861-896}$	$\delta_S^{896-931}$	$\delta_S^{931-966}$	$\delta_\parallel$	$\delta_\perp$	f_0	$f_\parallel$
A_S^{CP}	1.00	−0.09	−0.07	−0.27	−0.18	0.04	−0.01	−0.13	0.15	0.05	0.02	0.07	−0.01	−0.00	−0.01	−0.04
A_0^{CP}	−0.09	1.00	−0.16	−0.08	0.01	−0.02	−0.03	−0.02	−0.01	−0.03	−0.03	−0.02	0.01	0.02	0.01	−0.01
$A_\parallel^{CP}$	−0.07	−0.16	1.00	−0.57	−0.01	−0.04	−0.01	−0.02	−0.01	−0.05	−0.00	0.01	−0.03	−0.04	−0.01	0.01
$A_\perp^{CP}$	−0.27	−0.08	−0.57	1.00	0.06	−0.01	−0.03	0.04	−0.04	−0.00	−0.02	−0.02	0.01	0.02	0.01	0.04
$F_S^{826-861}$	−0.18	0.01	−0.01	0.06	1.00	0.00	0.02	0.04	−0.65	0.00	0.01	−0.02	−0.00	−0.03	−0.00	0.14
$F_S^{861-896}$	0.04	−0.02	−0.04	−0.01	0.00	1.00	0.03	−0.00	0.00	0.73	−0.01	−0.01	0.10	0.09	0.13	0.01
$F_S^{896-931}$	−0.01	−0.03	−0.01	−0.03	0.02	0.03	1.00	0.01	−0.02	0.02	0.29	−0.01	0.02	0.02	0.06	0.10
$F_S^{931-966}$	−0.13	−0.02	−0.02	0.04	0.04	−0.00	0.01	1.00	−0.03	0.01	0.01	−0.22	0.02	−0.02	−0.04	0.10
$\delta_S^{826-861}$	0.15	−0.01	−0.01	−0.04	−0.65	0.00	−0.02	−0.03	1.00	0.01	0.00	0.02	0.06	0.06	0.01	−0.14
$\delta_S^{861-896}$	0.05	−0.03	−0.05	−0.00	0.00	0.73	0.02	0.01	0.01	1.00	0.04	0.02	0.17	0.14	−0.04	0.08
$\delta_S^{896-931}$	0.02	−0.03	−0.00	−0.02	0.01	−0.01	0.29	0.01	0.00	0.04	1.00	0.05	0.15	0.12	−0.22	0.14
$\delta_S^{931-966}$	0.07	−0.02	0.01	−0.02	−0.02	−0.01	−0.01	−0.22	0.02	0.02	0.05	1.00	0.12	0.11	−0.14	0.02
$\delta_\parallel$	−0.01	0.01	−0.03	0.01	−0.00	0.10	0.02	0.02	0.06	0.17	0.15	0.12	1.00	0.69	−0.09	0.05
$\delta_\perp$	−0.00	0.02	−0.04	0.02	−0.03	0.09	0.02	−0.02	0.06	0.14	0.12	0.11	0.69	1.00	−0.03	0.00
f_0	−0.01	0.01	−0.01	0.01	−0.00	0.13	0.06	−0.04	0.01	−0.04	−0.22	−0.14	−0.09	−0.03	1.00	−0.44
$f_\parallel$	−0.04	−0.01	0.01	0.04	0.14	0.01	0.10	0.10	−0.14	0.08	0.14	0.02	0.05	0.00	−0.44	1.00

Table 5. Statistical correlation matrix for the physics parameters in the angular fit on $B_s^0 \to J/\psi \overline{K}^{*0}$ decays. The S-wave fraction and phase are allowed to vary freely in each of these $m_{K\pi}$ bins. These bin-dependent parameters are denoted using superscripts indicating the bin range, for example, $F_S^{826-861}$ and $\delta_S^{826-861}$ represent the S-wave fraction and phase, respectively, in the first $m_{K\pi}$ bin covering the range 826 to 861 MeV/c^2.

JHEP10(2025)173

Data Availability Statement. This article has associated data in a data repository. Data associated to the plots in this publication as well as in supplementary materials are made available on the CERN document server at https://cds.cern.ch/record/2936885.

Code Availability Statement. This article has no associated code or the code will not be deposited.

References

[1] LHCb collaboration, *Measurement of the CP-violating phase ϕ_s in the decay $B_s^0 \to J/\psi\phi$*, *Phys. Rev. Lett.* **108** (2012) 101803 [arXiv:1112.3183] [INSPIRE].

[2] K. De Bruyn, R. Fleischer, E. Malami and P. van Vliet, *New physics in B_q^0–$\bar{B}_q^0$ mixing: present challenges, prospects, and implications for $B_q^0 \to \mu^+\mu^-$*, *J. Phys. G* **50** (2023) 045003 [arXiv:2208.14910] [INSPIRE].

[3] I.I.Y. Bigi and A.I. Sanda, *Notes on the Observability of CP Violations in B Decays*, *Nucl. Phys. B* **193** (1981) 85 [INSPIRE].

[4] A.B. Carter and A.I. Sanda, *CP Violation in B Meson Decays*, *Phys. Rev. D* **23** (1981) 1567 [INSPIRE].

[5] A.B. Carter and A.I. Sanda, *CP Violation in Cascade Decays of B Mesons*, *Phys. Rev. Lett.* **45** (1980) 952 [INSPIRE].

[6] J. Charles et al., *Current status of the Standard Model CKM fit and constraints on $\Delta F = 2$ New Physics*, *Phys. Rev. D* **91** (2015) 073007 [arXiv:1501.05013] [INSPIRE].

[7] UTfit collaboration, *The unitarity triangle fit in the standard model and hadronic parameters from lattice QCD: A reappraisal after the measurements of Δm_s and $BR(B \to \tau\nu_\tau)$*, *JHEP* **10** (2006) 081 [hep-ph/0606167] [INSPIRE].

[8] Heavy Flavor Averaging Group (HFLAV) collaboration, *Averages of b-hadron, c-hadron, and τ-lepton properties as of 2023*, arXiv:2411.18639 [INSPIRE].

[9] C.-W. Chiang et al., *New physics in $B_s^0 \to J/\psi\phi$: a general analysis*, *JHEP* **04** (2010) 031 [arXiv:0910.2929] [INSPIRE].

[10] X. Liu, W. Wang and Y. Xie, *Penguin pollution in $B \to J/\psi V$ decays and impact on the extraction of the $B_s - \bar{B}_s$ mixing phase*, *Phys. Rev. D* **89** (2014) 094010 [arXiv:1309.0313] [INSPIRE].

[11] P. Frings, U. Nierste and M. Wiebusch, *Penguin contributions to CP phases in $B_{d,s}$ decays to charmonium*, *Phys. Rev. Lett.* **115** (2015) 061802 [arXiv:1503.00859] [INSPIRE].

[12] R. Fleischer, *Extracting CKM phases from angular distributions of $B_{d,s}$ decays into admixtures of CP eigenstates*, *Phys. Rev. D* **60** (1999) 073008 [hep-ph/9903540] [INSPIRE].

[13] S. Faller, R. Fleischer and T. Mannel, *Precision Physics with $B_s^0 \to J/\psi\phi$ at the LHC: The Quest for New Physics*, *Phys. Rev. D* **79** (2009) 014005 [arXiv:0810.4248] [INSPIRE].

[14] K. De Bruyn and R. Fleischer, *A Roadmap to Control Penguin Effects in $B_d^0 \to J/\psi K_S^0$ and $B_s^0 \to J/\psi\phi$*, *JHEP* **03** (2015) 145 [arXiv:1412.6834] [INSPIRE].

JHEP10(2025)173

[15] M.Z. Barel, K. De Bruyn, R. Fleischer and E. Malami, *In pursuit of new physics with $B_d^0 \to J/\psi K^0$ and $B_s^0 \to J/\psi\phi$ decays at the high-precision Frontier*, *J. Phys. G* **48** (2021) 065002 [arXiv:2010.14423] [INSPIRE].

[16] K. De Bruyn, R. Fleischer and E. Malami, *How to tame penguins: Advancing to high-precision measurements of ϕ_d and ϕ_s*, arXiv:2505.06102 [INSPIRE].

[17] LHCb collaboration, *Measurement of CP violation parameters and polarisation fractions in $B_s^0 \to J/\psi \overline{K}^{*0}$ decays*, *JHEP* **11** (2015) 082 [arXiv:1509.00400] [INSPIRE].

[18] LHCb collaboration, *Measurement of the CP-violating phase β in $B^0 \to J/\psi\pi^+\pi^-$ decays and limits on penguin effects*, *Phys. Lett. B* **742** (2015) 38 [arXiv:1411.1634] [INSPIRE].

[19] LHCb collaboration, *The LHCb Detector at the LHC*, 2008 *JINST* **3** S08005 [INSPIRE].

[20] LHCb collaboration, *LHCb Detector Performance*, *Int. J. Mod. Phys. A* **30** (2015) 1530022 [arXiv:1412.6352] [INSPIRE].

[21] R. Aaij et al., *Performance of the LHCb Vertex Locator*, 2014 *JINST* **9** P09007 [arXiv:1405.7808] [INSPIRE].

[22] LHCb Outer Tracker Group collaboration, *Improved performance of the LHCb Outer Tracker in LHC Run 2*, 2017 *JINST* **12** P11016 [arXiv:1708.00819] [INSPIRE].

[23] LHCb RICH Group collaboration, *Performance of the LHCb RICH detector at the LHC*, *Eur. Phys. J. C* **73** (2013) 2431 [arXiv:1211.6759] [INSPIRE].

[24] A.A. Alves Jr. et al., *Performance of the LHCb muon system*, 2013 *JINST* **8** P02022 [arXiv:1211.1346] [INSPIRE].

[25] T. Sjöstrand, S. Mrenna and P.Z. Skands, *A Brief Introduction to PYTHIA 8.1*, *Comput. Phys. Commun.* **178** (2008) 852 [arXiv:0710.3820] [INSPIRE].

[26] LHCb collaboration, *Handling of the generation of primary events in Gauss, the LHCb simulation framework*, *J. Phys. Conf. Ser.* **331** (2011) 032047 [INSPIRE].

[27] D.J. Lange, *The EvtGen particle decay simulation package*, *Nucl. Instrum. Meth. A* **462** (2001) 152 [INSPIRE].

[28] N. Davidson, T. Przedzinski and Z. Was, *PHOTOS interface in C++: Technical and Physics Documentation*, *Comput. Phys. Commun.* **199** (2016) 86 [arXiv:1011.0937] [INSPIRE].

[29] J. Allison et al., *Geant4 developments and applications*, *IEEE Trans. Nucl. Sci.* **53** (2006) 270 [INSPIRE].

[30] LHCb collaboration, *The LHCb simulation application, Gauss: Design, evolution and experience*, *J. Phys. Conf. Ser.* **331** (2011) 032023 [INSPIRE].

[31] A. Rogozhnikov, *Reweighting with Boosted Decision Trees*, *J. Phys. Conf. Ser.* **762** (2016) 012036 [arXiv:1608.05806] [INSPIRE].

[32] L. Anderlini et al., *The PIDCalib package*, LHCb-PUB-2016-021 (2016) [INSPIRE].

[33] R. Aaij et al., *Selection and processing of calibration samples to measure the particle identification performance of the LHCb experiment in Run 2*, *EPJ Tech. Instrum.* **6** (2019) 1 [arXiv:1803.00824] [INSPIRE].

[34] R. Aaij et al., *The LHCb Trigger and its Performance in 2011*, 2013 *JINST* **8** P04022 [arXiv:1211.3055] [INSPIRE].

[35] LHCb collaboration, *First observation of excited Ω_b^- states*, *Phys. Rev. Lett.* **124** (2020) 082002 [arXiv:2001.00851] [INSPIRE].

JHEP10(2025)173

[36] Particle Data Group collaboration, *Review of particle physics*, *Phys. Rev. D* **110** (2024) 030001 [INSPIRE].

[37] W.D. Hulsbergen, *Decay chain fitting with a Kalman filter*, *Nucl. Instrum. Meth. A* **552** (2005) 566 [physics/0503191] [INSPIRE].

[38] L. Breiman, J. Friedman, R.A. Olshen and C.J. Stone, *Classification and Regression Trees*, Chapman and Hall/CRC (2017) [DOI:10.1201/9781315139470] [INSPIRE].

[39] A. Blum, A. Kalai and J. Langford, *Beating the hold-out: bounds for k-fold and progressive cross-validation*, in *Proceedings of the Twelfth Annual Conference on Computational Learning Theory*, COLT '99, p. 203208, Association for Computing Machinery (1999), DOI.

[40] P. Koppenburg, *Statistical biases in measurements with multiple candidates*, arXiv:1703.01128 [INSPIRE].

[41] LHCb collaboration, *Measurement of the b-quark production cross-section in 7 and 13 TeV pp collisions*, *Phys. Rev. Lett.* **118** (2017) 052002 [*Erratum ibid.* **119** (2017) 169901] [arXiv:1612.05140] [INSPIRE].

[42] LHCb collaboration, *Precise measurement of the f_s/f_d ratio of fragmentation fractions and of B^0_s decay branching fractions*, *Phys. Rev. D* **104** (2021) 032005 [arXiv:2103.06810] [INSPIRE].

[43] LHCb collaboration, *Measurement of the resonant and CP components in $\overline{B}^0 \to J/\psi\pi^+\pi^-$ decays*, *Phys. Rev. D* **90** (2014) 012003 [arXiv:1404.5673] [INSPIRE].

[44] LHCb collaboration, *Amplitude analysis and the branching fraction measurement of $\bar{B}^0_s \to J/\psi K^+K^-$*, *Phys. Rev. D* **87** (2013) 072004 [arXiv:1302.1213] [INSPIRE].

[45] LHCb collaboration, *Observation of $J/\psi p$ Resonances Consistent with Pentaquark States in $\Lambda^0_b \to J/\psi K^- p$ Decays*, *Phys. Rev. Lett.* **115** (2015) 072001 [arXiv:1507.03414] [INSPIRE].

[46] M. De Cian, S. Farry, P. Seyfert and S. Stahl, *Fast neural-net based fake track rejection in the LHCb reconstruction*, LHCb-PUB-2017-011 (2017) [INSPIRE].

[47] M. Pivk and F.R. Le Diberder, *SPlot: A statistical tool to unfold data distributions*, *Nucl. Instrum. Meth. A* **555** (2005) 356 [physics/0402083] [INSPIRE].

[48] T. Skwarnicki, *A study of the radiative CASCADE transitions between the Upsilon-Prime and Upsilon resonances*, Ph.D. thesis, Cracow, INP, Poland (1986) [INSPIRE].

[49] R.N. Forthofer and R.G. Lehnen, *Rank correlation methods*, in *Public Program Analysis: A New Categorical Data Approach*, Springer US, Boston, MA, U.S.A. (1981), pp. 146–163, [DOI:10.1007/978-1-4684-6683-6_9].

[50] H. Dembinski, M. Kenzie, C. Langenbruch and M. Schmelling, *Custom Orthogonal Weight functions (COWs) for event classification*, *Nucl. Instrum. Meth. A* **1040** (2022) 167270 [arXiv:2112.04574] [INSPIRE].

[51] Y. Xie, *sFit: a method for background subtraction in maximum likelihood fit*, arXiv:0905.0724 [INSPIRE].

[52] L. Zhang and S. Stone, *Time-dependent Dalitz-plot formalism for $B_q \to J/\psi\ h^+h^-$*, *Phys. Lett. B* **719** (2013) 383 [arXiv:1212.6434] [INSPIRE].

[53] LHCb collaboration, *Updated measurement of time-dependent CP-violating observables in $B^0_s \to J/\psi K^+K^-$ decays*, *Eur. Phys. J. C* **79** (2019) 706 [*Erratum ibid.* **80** (2020) 601] [arXiv:1906.08356] [INSPIRE].

JHEP10(2025)173

[54] BaBar collaboration, *Measurement of the $B \to J/\psi K^*(892)$ decay amplitudes*, *Phys. Rev. Lett.* **87** (2001) 241801 [hep-ex/0107049] [INSPIRE].

[55] BaBar collaboration, *Ambiguity-free measurement of $\cos(2\beta)$: Time-integrated and time-dependent angular analyses of $B \to J/\psi K\pi$*, *Phys. Rev. D* **71** (2005) 032005 [hep-ex/0411016] [INSPIRE].

[56] B. Efron, *Bootstrap Methods: Another Look at the Jackknife*, *Annals Statist.* **7** (1979) 1 [INSPIRE].

[57] LHCb collaboration, *Measurement of B^0, B_s^0, B^+ and Λ_b^0 production asymmetries in 7 and 8 TeV proton-proton collisions*, *Phys. Lett. B* **774** (2017) 139 [arXiv:1703.08464] [INSPIRE].

[58] A. Davis et al., *Measurement of the instrumental asymmetry for $K^-\pi^+$-pairs at LHCb in Run 2*, LHCb-PUB-2018-004 (2018) [INSPIRE].

[59] Belle collaboration, *Measurements of branching fractions and decay amplitudes in $B \to J/\psi K^*$ decays*, *Phys. Lett. B* **538** (2002) 11 [hep-ex/0205021] [INSPIRE].

[60] D. Martínez Santos and F. Dupertuis, *Mass distributions marginalized over per-event errors*, *Nucl. Instrum. Meth. A* **764** (2014) 150 [arXiv:1312.5000] [INSPIRE].

[61] Belle collaboration, *Observation of a new charged charmoniumlike state in $\bar{B}^0 \to J/\psi K^-\pi^+$ decays*, *Phys. Rev. D* **90** (2014) 112009 [arXiv:1408.6457] [INSPIRE].

[62] R. Nisius, *BLUE: combining correlated estimates of physics observables within ROOT using the Best Linear Unbiased Estimate method*, arXiv:2001.10310 [DOI:10.1016/j.softx.2020.100468] [INSPIRE].

[63] LHCb collaboration, *Measurement of the fragmentation fraction ratio f_s/f_d and its dependence on B meson kinematics*, *JHEP* **04** (2013) 001 [arXiv:1301.5286] [INSPIRE].

JHEP10(2025)173

The LHCb collaboration

R. Aaij[38], A.S.W. Abdelmotteleb[57], C. Abellan Beteta[51], F. Abudinén[57], T. Ackernley[61], A.A. Adefisoye[69], B. Adeva[47], M. Adinolfi[55], P. Adlarson[85], C. Agapopoulou[14], C.A. Aidala[87], Z. Ajaltouni[11], S. Akar[11], K. Akiba[38], P. Albicocco[28], J. Albrecht[19,f], R. Aleksiejunas[80], F. Alessio[49], Z. Aliouche[63], P. Alvarez Cartelle[56], R. Amalric[16], S. Amato[3], J.L. Amey[55], Y. Amhis[14], L. An[6], L. Anderlini[27], M. Andersson[51], P. Andreola[51], M. Andreotti[26], S. Andres Estrada[84], A. Anelli[31,o,49], D. Ao[7], F. Archilli[37,v], Z Areg[69], M. Argenton[26], S. Arguedas Cuendis[9,49], A. Artamonov[44], M. Artuso[69], E. Aslanides[13], R. Ataíde Da Silva[50], M. Atzeni[65], B. Audurier[12], J.A. Authier[15], D. Bacher[64], I. Bachiller Perea[50], S. Bachmann[22], M. Bachmayer[50], J.J. Back[57], P. Baladron Rodriguez[47], V. Balagura[15], A. Balboni[26], W. Baldini[26], L. Balzani[19], H. Bao[7], J. Baptista de Souza Leite[61], C. Barbero Pretel[47,12], M. Barbetti[27], I.R. Barbosa[70], R.J. Barlow[63], M. Barnyakov[25], S. Barsuk[14], W. Barter[59], J. Bartz[69], S. Bashir[40], B. Batsukh[5], P.B. Battista[14], A. Bay[50], A. Beck[65], M. Becker[19], F. Bedeschi[35], I.B. Bediaga[2], N.A. Behling[19], S. Belin[47], K. Belous[44], I. Belov[29], I. Belyaev[36], G. Benane[13], G. Bencivenni[28], E. Ben-Haim[16], A. Berezhnoy[44], R. Bernet[51], S. Bernet Andres[46], A. Bertolin[33], C. Betancourt[51], F. Betti[59], J. Bex[56], Ia. Bezshyiko[51], O. Bezshyyko[86], J. Bhom[41], M.S. Bieker[18], N.V. Biesuz[26], P. Billoir[16], A. Biolchini[38], M. Birch[62], F.C.R. Bishop[10], A. Bitadze[63], A. Bizzeti[27,p], T. Blake[57,b], F. Blanc[50], J.E. Blank[19], S. Blusk[69], V. Bocharnikov[44], J.A. Boelhauve[19], O. Boente Garcia[15], T. Boettcher[68], A. Bohare[59], A. Boldyrev[44], C.S. Bolognani[82], R. Bolzonella[26,l], R.B. Bonacci[1], N. Bondar[44,49], A. Bordelius[49], F. Borgato[33,49], S. Borghi[63], M. Borsato[31,o], J.T. Borsuk[83], E. Bottalico[61], S.A. Bouchiba[50], M. Bovill[64], T.J.V. Bowcock[61], A. Boyer[49], C. Bozzi[26], J.D. Brandenburg[88], A. Brea Rodriguez[50], N. Breer[19], J. Brodzicka[41], A. Brossa Gonzalo[47,†], J. Brown[61], D. Brundu[32], E. Buchanan[59], L. Buonincontri[33,q], M. Burgos Marcos[82], A.T. Burke[63], C. Burr[49], J.S. Butter[56], J. Buytaert[49], W. Byczynski[49], S. Cadeddu[32], H. Cai[75], Y. Cai[5], A. Caillet[16], R. Calabrese[26,l], S. Calderon Ramirez[9], L. Calefice[45], S. Cali[28], M. Calvi[31,o], M. Calvo Gomez[46], P. Camargo Magalhaes[2,aa], J.I. Cambon Bouzas[47], P. Campana[28], D.H. Campora Perez[82], A.F. Campoverde Quezada[7], S. Capelli[31], L. Capriotti[26], R. Caravaca-Mora[9], A. Carbone[25,j], L. Carcedo Salgado[47], R. Cardinale[29,m], A. Cardini[32], P. Carniti[31], L. Carus[22], A. Casais Vidal[65], R. Caspary[22], G. Casse[61], M. Cattaneo[49], G. Cavallero[26], V. Cavallini[26,l], S. Celani[22], S. Cesare[30,n], F. Cesario Laterza Lopes[2], A.J. Chadwick[61], I. Chahrour[87], H. Chang[4,c], M. Charles[16], Ph. Charpentier[49], E. Chatzianagnostou[38], R. Cheaib[79], M. Chefdeville[10], C. Chen[56], J. Chen[50], S. Chen[5], Z. Chen[7], M. Cherif[12], A. Chernov[41], S. Chernyshenko[53], X. Chiotopoulos[82], V. Chobanova[84], M. Chrzaszcz[41], A. Chubykin[44], V. Chulikov[28,36], P. Ciambrone[28], X. Cid Vidal[47], G. Ciezarek[49], P. Cifra[38], P.E.L. Clarke[59], M. Clemencic[49], H.V. Cliff[56], J. Closier[49], C. Cocha Toapaxi[22], V. Coco[49], J. Cogan[13], E. Cogneras[11], L. Cojocariu[43], S. Collaviti[50], P. Collins[49], T. Colombo[49], M. Colonna[19], A. Comerma-Montells[45], L. Congedo[24], J. Connaughton[57], A. Contu[32], N. Cooke[60], C. Coronel[66], I. Corredoira [12], A. Correia[16], G. Corti[49], J. Cottee Meldrum[55], B. Couturier[49], D.C. Craik[51], M. Cruz Torres[2,g], E. Curras Rivera[50],

JHEP10(2025)173

R. Currie[59], C.L. Da Silva[68], S. Dadabaev[44], L. Dai[72], X. Dai[4], E. Dall'Occo[49], J. Dalseno[84], C. D'Ambrosio[62], J. Daniel[11], P. d'Argent[24], G. Darze[3], A. Davidson[57], J.E. Davies[63], O. De Aguiar Francisco[63], C. De Angelis[32,k], F. De Benedetti[49], J. de Boer[38], K. De Bruyn[81], S. De Capua[63], M. De Cian[63], U. De Freitas Carneiro Da Graca[2,a], E. De Lucia[28], J.M. De Miranda[2], L. De Paula[3], M. De Serio[24,h], P. De Simone[28], F. De Vellis[19], J.A. de Vries[82], F. Debernardis[24], D. Decamp[10], S. Dekkers[1], L. Del Buono[16], B. Delaney[65], H.-P. Dembinski[19], J. Deng[8], V. Denysenko[51], O. Deschamps[11], F. Dettori[32,k], B. Dey[79], P. Di Nezza[28], I. Diachkov[44], S. Didenko[44], S. Ding[69], Y. Ding[50], L. Dittmann[22], V. Dobishuk[53], A.D. Docheva[60], A. Doheny[57], C. Dong[4,c], A.M. Donohoe[23], F. Dordei[32], A.C. dos Reis[2], A.D. Dowling[69], L. Dreyfus[13], W. Duan[73], P. Duda[83], M.W. Dudek[41], L. Dufour[49], V. Duk[34], P. Durante[49], M.M. Duras[83], J.M. Durham[68], O.D. Durmus[79], A. Dziurda[41], A. Dzyuba[44], S. Easo[58], E. Eckstein[18], U. Egede[1], A. Egorychev[44], V. Egorychev[44], S. Eisenhardt[59], E. Ejopu[63], L. Eklund[85], M. Elashri[66], J. Ellbracht[19], S. Ely[62], A. Ene[43], J. Eschle[69], S. Esen[22], T. Evans[38], F. Fabiano[32], S. Faghih[66], L.N. Falcao[2], B. Fang[7], R. Fantechi[35], L. Fantini[34,r], M. Faria[50], K. Farmer[59], D. Fazzini[31,o], L. Felkowski[83], M. Feng[5,7], M. Feo[19], A. Fernandez Casani[48], M. Fernandez Gomez[47], A.D. Fernez[67], F. Ferrari[25,j], F. Ferreira Rodrigues[3], M. Ferrillo[51], M. Ferro-Luzzi[49], S. Filippov[44], R.A. Fini[24], M. Fiorini[26,l], M. Firlej[40], K.L. Fischer[64], D.S. Fitzgerald[87], C. Fitzpatrick[63], T. Fiutowski[40], F. Fleuret[15], A. Fomin[52], M. Fontana[25], L.F. Foreman[63], R. Forty[49], D. Foulds-Holt[59], V. Franco Lima[3], M. Franco Sevilla[67], M. Frank[49], E. Franzoso[26,l], G. Frau[63], C. Frei[49], D.A. Friday[63], J. Fu[7], Q. Führing[19,f,56], T. Fulghesu[13], G. Galati[24], M.D. Galati[38], A. Gallas Torreira[47], D. Galli[25,j], S. Gambetta[59], M. Gandelman[3], P. Gandini[30], B. Ganie[63], H. Gao[7], R. Gao[64], T.Q. Gao[56], Y. Gao[8], Y. Gao[6], Y. Gao[8], L.M. Garcia Martin[50], P. Garcia Moreno[45], J. García Pardiñas[65], P. Gardner[67], K.G. Garg[8], L. Garrido[45], C. Gaspar[49], A. Gavrikov[33], L.L. Gerken[19], E. Gersabeck[20], M. Gersabeck[20], T. Gershon[57], S. Ghizzo[29,m], Z. Ghorbanimoghaddam[55], L. Giambastiani[33,q], F.I. Giasemis[16,e], V. Gibson[56], H.K. Giemza[42], A.L. Gilman[64], M. Giovannetti[28], A. Gioventù[45], L. Girardey[63,58], M.A. Giza[41], F.C. Glaser[14,22], V.V. Gligorov[16], C. Göbel[70], L. Golinka-Bezshyyko[86], E. Golobardes[46], D. Golubkov[44], A. Golutvin[62,49], S. Gomez Fernandez[45], W. Gomulka[40], I. Gonçales Vaz[49], F. Goncalves Abrantes[64], M. Goncerz[41], G. Gong[4,c], J.A. Gooding[19], I.V. Gorelov[44], C. Gotti[31], E. Govorkova[65], J.P. Grabowski[18], L.A. Granado Cardoso[49], E. Graugés[45], E. Graverini[50,t], L. Grazette[57], G. Graziani[27], A.T. Grecu[43], L.M. Greeven[38], N.A. Grieser[66], L. Grillo[60], S. Gromov[44], C. Gu[15], M. Guarise[26], L. Guerry[11], V. Guliaeva[44], P.A. Günther[22], A.-K. Guseinov[50], E. Gushchin[44], Y. Guz[6,49], T. Gys[49], K. Habermann[18], T. Hadavizadeh[1], C. Hadjivasiliou[67], G. Haefeli[50], C. Haen[49], S. Haken[56], G. Hallett[57], P.M. Hamilton[67], J. Hammerich[61], Q. Han[33], X. Han[22,49], S. Hansmann-Menzemer[22], L. Hao[7], N. Harnew[64], T.H. Harris[1], M. Hartmann[14], S. Hashmi[40], J. He[7,d], A. Hedes[63], F. Hemmer[49], C. Henderson[66], R. Henderson[14], R.D.L. Henderson[1], A.M. Hennequin[49], K. Hennessy[61], L. Henry[50], J. Herd[62], P. Herrero Gascon[22], J. Heuel[17], A. Hicheur[3], G. Hijano Mendizabal[51], J. Horswill[63], R. Hou[8], Y. Hou[11], D.C. Houston[60],

JHEP10(2025)173

N. Howarth[61], J. Hu[73], W. Hu[7], X. Hu[4,c], W. Hulsbergen[38], R.J. Hunter[57], M. Hushchyn[44], D. Hutchcroft[61], M. Idzik[40], D. Ilin[44], P. Ilten[66], A. Iniukhin[44], A. Iohner[10], A. Ishteev[44], K. Ivshin[44], H. Jage[17], S.J. Jaimes Elles[77,49,48], S. Jakobsen[49], E. Jans[38], B.K. Jashal[48], A. Jawahery[67], C. Jayaweera[54], V. Jevtic[19], Z. Jia[16], E. Jiang[67], X. Jiang[5,7], Y. Jiang[7], Y.J. Jiang[6], E. Jimenez Moya[9], N. Jindal[88], M. John[64], A. John Rubesh Rajan[23], D. Johnson[54], C.R. Jones[56], S. Joshi[42], B. Jost[49], J. Juan Castella[56], N. Jurik[49], I. Juszczak[41], D. Kaminaris[50], S. Kandybei[52], M. Kane[59], Y. Kang[4,c], C. Kar[11], M. Karacson[49], A. Kauniskangas[50], J.W. Kautz[66], M.K. Kazanecki[41], F. Keizer[49], M. Kenzie[56], T. Ketel[38], B. Khanji[69], A. Kharisova[44], S. Kholodenko[35,49], G. Khreich[14], T. Kirn[17], V.S. Kirsebom[31,o], O. Kitouni[65], S. Klaver[39], N. Kleijne[35,s], D.K. Klekots[86], K. Klimaszewski[42], M.R. Kmiec[42], S. Koliiev[53], L. Kolk[19], A. Konoplyannikov[6], P. Kopciewicz[49], P. Koppenburg[38], A. Korchin[52], M. Korolev[44], I. Kostiuk[38], O. Kot[53], S. Kotriakhova, E. Kowalczyk[67], A. Kozachuk[44], P. Kravchenko[44], L. Kravchuk[44], O. Kravcov[80], M. Kreps[57], P. Krokovny[44], W. Krupa[69], W. Krzemien[42], O. Kshyvanskyi[53], S. Kubis[83], M. Kucharczyk[41], V. Kudryavtsev[44], E. Kulikova[44], A. Kupsc[85], V. Kushnir[52], B. Kutsenko[13], I. Kyryllin[52], D. Lacarrere[49], P. Laguarta Gonzalez[45], A. Lai[32], A. Lampis[32], D. Lancierini[62], C. Landesa Gomez[47], J.J. Lane[1], G. Lanfranchi[28], C. Langenbruch[22], J. Langer[19], O. Lantwin[44], T. Latham[57], F. Lazzari[35,t,49], C. Lazzeroni[54], R. Le Gac[13], H. Lee[61], R. Lefèvre[11], A. Leflat[44], S. Legotin[44], M. Lehuraux[57], E. Lemos Cid[49], O. Leroy[13], T. Lesiak[41], E.D. Lesser[49], B. Leverington[22], A. Li[4,c], C. Li[4], C. Li[13], H. Li[73], J. Li[8], K. Li[76], L. Li[63], M. Li[8], P. Li[7], P.-R. Li[74], Q. Li[5,7], T. Li[72], T. Li[73], Y. Li[8], Y. Li[5], Y. Li[4], Z. Lian[4,c], Q. Liang[8], X. Liang[69], Z. Liang[32], S. Libralon[48], A.L. Lightbody[12], C. Lin[7], T. Lin[58], R. Lindner[49], H. Linton[62], R. Litvinov[32], D. Liu[8], F.L. Liu[1], G. Liu[73], K. Liu[74], S. Liu[5,7], W. Liu[8], Y. Liu[59], Y. Liu[74], Y.L. Liu[62], G. Loachamin Ordonez[70], A. Lobo Salvia[45], A. Loi[32], T. Long[56], J.H. Lopes[3], A. Lopez Huertas[45], C. Lopez Iribarnegaray[47], S. López Soliño[47], Q. Lu[15], C. Lucarelli[49], D. Lucchesi[33,q], M. Lucio Martinez[48], Y. Luo[6], A. Lupato[33,i], E. Luppi[26,l], K. Lynch[23], X.-R. Lyu[7], G.M. Ma[4,c], S. Maccolini[19], F. Machefert[14], F. Maciuc[43], B. Mack[69], I. Mackay[64], L.M. Mackey[69], L.R. Madhan Mohan[56], M.J. Madurai[54], D. Magdalinski[38], D. Maisuzenko[44], J.J. Malczewski[41], S. Malde[64], L. Malentacca[49], A. Malinin[44], T. Maltsev[44], G. Manca[32,k], G. Mancinelli[13], C. Mancuso[14], R. Manera Escalero[45], F.M. Manganella[37], D. Manuzzi[25], D. Marangotto[30,n], J.F. Marchand[10], R. Marchevski[50], U. Marconi[25], E. Mariani[16], S. Mariani[49], C. Marin Benito[45], J. Marks[22], A.M. Marshall[55], L. Martel[64], G. Martelli[34], G. Martellotti[36], L. Martinazzoli[49], M. Martinelli[31,o], D. Martinez Gomez[81], D. Martinez Santos[84], F. Martinez Vidal[48], A. Martorell i Granollers[46], A. Massafferri[2], R. Matev[49], A. Mathad[49], V. Matiunin[44], C. Matteuzzi[69], K.R. Mattioli[15], A. Mauri[62], E. Maurice[15], J. Mauricio[45], P. Mayencourt[50], J. Mazorra de Cos[48], M. Mazurek[42], M. McCann[62], T.H. McGrath[63], N.T. McHugh[60], A. McNab[63], R. McNulty[23], B. Meadows[66], G. Meier[19], D. Melnychuk[42], D. Mendoza Granada[16], F.M. Meng[4,c], M. Merk[38,82], A. Merli[50,30], L. Meyer Garcia[67], D. Miao[5,7], H. Miao[7], M. Mikhasenko[78], D.A. Milanes[77,y],

JHEP10(2025)173

A. Minotti[31,o], E. Minucci[28], T. Miralles[11], B. Mitreska[19], D.S. Mitzel[19], A. Modak[58], L. Moeser[19], R.D. Moise[17], E.F. Molina Cardenas[87], T. Mombächer[49], M. Monk[57,1], S. Monteil[11], A. Morcillo Gomez[47], G. Morello[28], M.J. Morello[35,s], M.P. Morgenthaler[22], J. Moron[40], W. Morren[38], A.B. Morris[49], A.G. Morris[13], R. Mountain[69], H. Mu[4,c], Z.M. Mu[6], E. Muhammad[57], F. Muheim[59], M. Mulder[81], K. Müller[51], F. Muñoz-Rojas[9], R. Murta[62], V. Mytrochenko[52], P. Naik[61], T. Nakada[50], R. Nandakumar[58], T. Nanut[49], I. Nasteva[3], M. Needham[59], E. Nekrasova[44], N. Neri[30,n], S. Neubert[18], N. Neufeld[49], P. Neustroev[44], J. Nicolini[49], D. Nicotra[82], E.M. Niel[15], N. Nikitin[44], Q. Niu[74], P. Nogarolli[3], P. Nogga[18], C. Normand[55], J. Novoa Fernandez[47], G. Nowak[66], C. Nunez[87], H.N. Nur[60], A. Oblakowska-Mucha[40], V. Obraztsov[44], T. Oeser[17], A. Okhotnikov[44], O. Okhrimenko[53], R. Oldeman[32,k], F. Oliva[59,49], E. Olivart Pino[45], M. Olocco[19], C.J.G. Onderwater[82], R.H. O'Neil[49], J.S. Ordonez Soto[11], D. Osthues[19], J.M. Otalora Goicochea[3], P. Owen[51], A. Oyanguren[48], O. Ozcelik[49], F. Paciolla[35,w], A. Padee[42], K.O. Padeken[18], B. Pagare[47], T. Pajero[49], A. Palano[24], M. Palutan[28], C. Pan[75], X. Pan[4,c], S. Panebianco[12], G. Panshin[5], L. Paolucci[57], A. Papanestis[58], M. Pappagallo[24,h], L.L. Pappalardo[26], C. Pappenheimer[66], C. Parkes[63], D. Parmar[78], B. Passalacqua[26,l], G. Passaleva[27], D. Passaro[35,s,49], A. Pastore[24], M. Patel[62], J. Patoc[64], C. Patrignani[25,j], A. Paul[69], C.J. Pawley[82], A. Pellegrino[38], J. Peng[5,7], X. Peng[74], M. Pepe Altarelli[28], S. Perazzini[25], D. Pereima[44], H. Pereira Da Costa[68], M. Pereira Martinez[47], A. Pereiro Castro[47], C. Perez[46], P. Perret[11], A. Perrevoort[81], A. Perro[49,13], M.J. Peters[66], K. Petridis[55], A. Petrolini[29,m], J.P. Pfaller[66], H. Pham[69], L. Pica[35,s], M. Piccini[34], L. Piccolo[32], B. Pietrzyk[10], G. Pietrzyk[14], R.N. Pilato[61], D. Pinci[36], F. Pisani[49], M. Pizzichemi[31,o,49], V.M. Placinta[43], M. Plo Casasus[47], T. Poeschl[49], F. Polci[16], M. Poli Lener[28], A. Poluektov[13], N. Polukhina[44], I. Polyakov[63], E. Polycarpo[3], S. Ponce[49], D. Popov[7,49], S. Poslavskii[44], K. Prasanth[59], C. Prouve[84], D. Provenzano[32,k,49], V. Pugatch[53], G. Punzi[35,t], J.R. Pybus[68], S. Qasim[51], Q.Q. Qian[6], W. Qian[7], N. Qin[4,c], S. Qu[4,c], R. Quagliani[49], R.I. Rabadan Trejo[57], R. Racz[80], J.H. Rademacker[55], M. Rama[35], M. Ramírez García[87], V. Ramos De Oliveira[70], M. Ramos Pernas[57], M.S. Rangel[3], F. Ratnikov[44], G. Raven[39], M. Rebollo De Miguel[48], F. Redi[30,i], J. Reich[55], F. Reiss[20], Z. Ren[7], P.K. Resmi[64], M. Ribalda Galvez[45], R. Ribatti[50], G. Ricart[15,12], D. Riccardi[35,s], S. Ricciardi[58], K. Richardson[65], M. Richardson-Slipper[56], K. Rinnert[61], P. Robbe[14,49], G. Robertson[60], E. Rodrigues[61], A. Rodriguez Alvarez[45], E. Rodriguez Fernandez[47], J.A. Rodriguez Lopez[77], E. Rodriguez Rodriguez[49], J. Roensch[19], A. Rogachev[44], A. Rogovskiy[58], D.L. Rolf[19], P. Roloff[49], V. Romanovskiy[66], A. Romero Vidal[47], G. Romolini[26,49], F. Ronchetti[50], T. Rong[6], M. Rotondo[28], S.R. Roy[22], M.S. Rudolph[69], M. Ruiz Diaz[22], R.A. Ruiz Fernandez[47], J. Ruiz Vidal[82], J.J. Saavedra-Arias[9], J.J. Saborido Silva[47], S.E.R. Sacha Emile R.[49], R. Sadek[15], N. Sagidova[44], D. Sahoo[79], N. Sahoo[54], B. Saitta[32,k], M. Salomoni[31,49,o], I. Sanderswood[48], R. Santacesaria[36], C. Santamarina Rios[47], M. Santimaria[28], L. Santoro[2], E. Santovetti[37], A. Saputi, D. Saranin[44], A. Sarnatskiy[81], G. Sarpis[49], M. Sarpis[80], C. Satriano[36,u], M. Saur[74], D. Savrina[44], H. Sazak[17], F. Sborzacchi[49,28], A. Scarabotto[19], S. Schael[17], S. Scherl[61], M. Schiller[22], H. Schindler[49], M. Schmelling[21], B. Schmidt[49], S. Schmitt[17], H. Schmitz[18],

JHEP10(2025)173

O. Schneider[50], A. Schopper[62], N. Schulte[19], M.H. Schune[14], G. Schwering[17], B. Sciascia[28], A. Sciuccati[49], I. Segal[78], S. Sellam[47], A. Semennikov[44], T. Senger[51], M. Senghi Soares[39], A. Sergi[29,m], N. Serra[51], L. Sestini[27], A. Seuthe[19], B. Sevilla Sanjuan[46], Y. Shang[6], D.M. Shangase[87], M. Shapkin[44], R.S. Sharma[69], I. Shchemerov[44], L. Shchutska[50], T. Shears[61], L. Shekhtman[44], Z. Shen[38], S. Sheng[5,7], V. Shevchenko[44], B. Shi[7], Q. Shi[7], W.S. Shi[73], Y. Shimizu[14], E. Shmanin[25], R. Shorkin[44], J.D. Shupperd[69], R. Silva Coutinho[69], G. Simi[33,q], S. Simone[24,h], M. Singha[79], N. Skidmore[57], T. Skwarnicki[69], M.W. Slater[54], E. Smith[65], K. Smith[68], M. Smith[62], L. Soares Lavra[59], M.D. Sokoloff[66], F.J.P. Soler[60], A. Solomin[55], A. Solovev[44], N.S. Sommerfeld[18], R. Song[1], Y. Song[50], Y. Song[4,c], Y.S. Song[6], F.L. Souza De Almeida[69], B. Souza De Paula[3], E. Spadaro Norella[29,m], E. Spedicato[25], J.G. Speer[19], P. Spradlin[60], V. Sriskaran[49], F. Stagni[49], M. Stahl[78], S. Stahl[49], S. Stanislaus[64], M. Stefaniak[88], E.N. Stein[49], O. Steinkamp[51], H. Stevens[19], D. Strekalina[44], Y. Su[7], F. Suljik[64], J. Sun[32], J. Sun[63], L. Sun[75], D. Sundfeld[2], W. Sutcliffe[51], V. Svintozelskyi[48], K. Swientek[40], F. Swystun[56], A. Szabelski[42], T. Szumlak[40], Y. Tan[4,c], Y. Tang[75], Y.T. Tang[7], M.D. Tat[22], J.A. Teijeiro Jimenez[47], A. Terentev[44], F. Terzuoli[35,w], F. Teubert[49], E. Thomas[49], D.J.D. Thompson[54], A.R. Thomson-Strong[59], H. Tilquin[62], V. Tisserand[11], S. T'Jampens[10], M. Tobin[5], T.T. Todorov[20], L. Tomassetti[26,l], G. Tonani[30], X. Tong[6], T. Tork[30], D. Torres Machado[2], L. Toscano[19], D.Y. Tou[4,c], C. Trippl[46], G. Tuci[22], N. Tuning[38], L.H. Uecker[22], A. Ukleja[40], D.J. Unverzagt[22], A. Upadhyay[49], B. Urbach[59], A. Usachov[39], A. Ustyuzhanin[44], U. Uwer[22], V. Vagnoni[25], V. Valcarce Cadenas[47], G. Valenti[25], N. Valls Canudas[49], J. van Eldik[49], H. Van Hecke[68], E. van Herwijnen[62], C.B. Van Hulse[47,z], R. Van Laak[50], M. van Veghel[38], G. Vasquez[51], R. Vazquez Gomez[45], P. Vazquez Regueiro[47], C. Vázquez Sierra[84], S. Vecchi[26], J. Velilla Serna[48], J.J. Velthuis[55], M. Veltri[27,x], A. Venkateswaran[50], M. Verdoglia[32], M. Vesterinen[57], W. Vetens[69], D. Vico Benet[64], P. Vidrier Villalba[45], M. Vieites Diaz[47], X. Vilasis-Cardona[46], E. Vilella Figueras[61], A. Villa[25], P. Vincent[16], B. Vivacqua[3], F.C. Volle[54], D. vom Bruch[13], N. Voropaev[44], K. Vos[82], C. Vrahas[59], J. Wagner[19], J. Walsh[35], E.J. Walton[1,57], G. Wan[6], A. Wang[7], B. Wang[5], C. Wang[22], G. Wang[8], H. Wang[74], J. Wang[6], J. Wang[5], J. Wang[4,c], J. Wang[75], M. Wang[49], N.W. Wang[7], R. Wang[55], X. Wang[8], X. Wang[73], X.W. Wang[62], Y. Wang[76], Y. Wang[6], Y.W. Wang[74], Z. Wang[14], Z. Wang[4,c], Z. Wang[30], J.A. Ward[57], M. Waterlaat[49], N.K. Watson[54], D. Websdale[62], Y. Wei[6], J. Wendel[84], B.D.C. Westhenry[55], C. White[56], M. Whitehead[60], E. Whiter[54], A.R. Wiederhold[63], D. Wiedner[19], M.A. Wiegertjes[38], C. Wild[64], G. Wilkinson[64,49], M.K. Wilkinson[66], M. Williams[65], M.J. Williams[49], M.R.J. Williams[59], R. Williams[56], S. Williams[55], Z. Williams[55], F.F. Wilson[58], M. Winn[12], W. Wislicki[42], M. Witek[41], L. Witola[19], T. Wolf[22], E. Wood[56], G. Wormser[14], S.A. Wotton[56], H. Wu[69], J. Wu[8,*], X. Wu[75], Y. Wu[6,56], Z. Wu[7], K. Wyllie[49], S. Xian[73], Z. Xiang[5], Y. Xie[8], T.X. Xing[30], A. Xu[35,s], L. Xu[4,c], L. Xu[4,c], M. Xu[49], Z. Xu[49], Z. Xu[7], Z. Xu[5], K. Yang[62], X. Yang[6], Y. Yang[15], Z. Yang[6], V. Yeroshenko[14], H. Yeung[63], H. Yin[8], X. Yin[7], C.Y. Yu[6], J. Yu[72], X. Yuan[5], Y Yuan[5,7], E. Zaffaroni[50], J.A. Zamora Saa[71], M. Zavertyaev[21], M. Zdybal[41],

JHEP10(2025)173

F. Zenesini[25], C. Zeng[5,7], M. Zeng[4,c], C. Zhang[6], D. Zhang[8], J. Zhang[7], L. Zhang[4,c], R. Zhang[8], S. Zhang[72], S. Zhang[64], Y. Zhang[6], Y.Z. Zhang[4,c], Z. Zhang[4,c], Y. Zhao[22], A. Zhelezov[22], S.Z. Zheng[6], X.Z. Zheng[4,c], Y. Zheng[7], T. Zhou[6], X. Zhou[8], Y. Zhou[7], V. Zhovkovska[57], L.Z. Zhu[7], X. Zhu[4,c], X. Zhu[8], Y. Zhu[17], V. Zhukov[17], J. Zhuo[48], Q. Zou[5,7], D. Zuliani[33,q], G. Zunica[50]

[1] *School of Physics and Astronomy, Monash University, Melbourne, Australia*
[2] *Centro Brasileiro de Pesquisas Físicas (CBPF), Rio de Janeiro, Brazil*
[3] *Universidade Federal do Rio de Janeiro (UFRJ), Rio de Janeiro, Brazil*
[4] *Department of Engineering Physics, Tsinghua University, Beijing, China*
[5] *Institute Of High Energy Physics (IHEP), Beijing, China*
[6] *School of Physics State Key Laboratory of Nuclear Physics and Technology, Peking University, Beijing, China*
[7] *University of Chinese Academy of Sciences, Beijing, China*
[8] *Institute of Particle Physics, Central China Normal University, Wuhan, Hubei, China*
[9] *Consejo Nacional de Rectores (CONARE), San Jose, Costa Rica*
[10] *Université Savoie Mont Blanc, CNRS, IN2P3-LAPP, Annecy, France*
[11] *Université Clermont Auvergne, CNRS/IN2P3, LPC, Clermont-Ferrand, France*
[12] *Université Paris-Saclay, Centre d'Etudes de Saclay (CEA), IRFU, Saclay, France, Gif-Sur-Yvette, France*
[13] *Aix Marseille Univ, CNRS/IN2P3, CPPM, Marseille, France*
[14] *Université Paris-Saclay, CNRS/IN2P3, IJCLab, Orsay, France*
[15] *Laboratoire Leprince-Ringuet, CNRS/IN2P3, Ecole Polytechnique, Institut Polytechnique de Paris, Palaiseau, France*
[16] *LPNHE, Sorbonne Université, Paris Diderot Sorbonne Paris Cité, CNRS/IN2P3, Paris, France*
[17] *I. Physikalisches Institut, RWTH Aachen University, Aachen, Germany*
[18] *Universität Bonn — Helmholtz-Institut für Strahlen und Kernphysik, Bonn, Germany*
[19] *Fakultät Physik, Technische Universität Dortmund, Dortmund, Germany*
[20] *Physikalisches Institut, Albert-Ludwigs-Universität Freiburg, Freiburg, Germany*
[21] *Max-Planck-Institut für Kernphysik (MPIK), Heidelberg, Germany*
[22] *Physikalisches Institut, Ruprecht-Karls-Universität Heidelberg, Heidelberg, Germany*
[23] *School of Physics, University College Dublin, Dublin, Ireland*
[24] *INFN Sezione di Bari, Bari, Italy*
[25] *INFN Sezione di Bologna, Bologna, Italy*
[26] *INFN Sezione di Ferrara, Ferrara, Italy*
[27] *INFN Sezione di Firenze, Firenze, Italy*
[28] *INFN Laboratori Nazionali di Frascati, Frascati, Italy*
[29] *INFN Sezione di Genova, Genova, Italy*
[30] *INFN Sezione di Milano, Milano, Italy*
[31] *INFN Sezione di Milano-Bicocca, Milano, Italy*
[32] *INFN Sezione di Cagliari, Monserrato, Italy*
[33] *INFN Sezione di Padova, Padova, Italy*
[34] *INFN Sezione di Perugia, Perugia, Italy*
[35] *INFN Sezione di Pisa, Pisa, Italy*
[36] *INFN Sezione di Roma La Sapienza, Roma, Italy*
[37] *INFN Sezione di Roma Tor Vergata, Roma, Italy*
[38] *Nikhef National Institute for Subatomic Physics, Amsterdam, Netherlands*
[39] *Nikhef National Institute for Subatomic Physics and VU University Amsterdam, Amsterdam, Netherlands*
[40] *AGH — University of Krakow, Faculty of Physics and Applied Computer Science, Kraków, Poland*
[41] *Henryk Niewodniczanski Institute of Nuclear Physics Polish Academy of Sciences, Kraków, Poland*
[42] *National Center for Nuclear Research (NCBJ), Warsaw, Poland*
[43] *Horia Hulubei National Institute of Physics and Nuclear Engineering, Bucharest-Magurele, Romania*
[44] *Authors affiliated with an institute formerly covered by a cooperation agreement with CERN.*
[45] *ICCUB, Universitat de Barcelona, Barcelona, Spain*

JHEP10(2025)173

[46] La Salle, Universitat Ramon Llull, Barcelona, Spain
[47] Instituto Galego de Física de Altas Enerxías (IGFAE), Universidade de Santiago de Compostela, Santiago de Compostela, Spain
[48] Instituto de Fisica Corpuscular, Centro Mixto Universidad de Valencia — CSIC, Valencia, Spain
[49] European Organization for Nuclear Research (CERN), Geneva, Switzerland
[50] Institute of Physics, Ecole Polytechnique Fédérale de Lausanne (EPFL), Lausanne, Switzerland
[51] Physik-Institut, Universität Zürich, Zürich, Switzerland
[52] NSC Kharkiv Institute of Physics and Technology (NSC KIPT), Kharkiv, Ukraine
[53] Institute for Nuclear Research of the National Academy of Sciences (KINR), Kyiv, Ukraine
[54] School of Physics and Astronomy, University of Birmingham, Birmingham, U.K.
[55] H.H. Wills Physics Laboratory, University of Bristol, Bristol, U.K.
[56] Cavendish Laboratory, University of Cambridge, Cambridge, U.K.
[57] Department of Physics, University of Warwick, Coventry, U.K.
[58] STFC Rutherford Appleton Laboratory, Didcot, U.K.
[59] School of Physics and Astronomy, University of Edinburgh, Edinburgh, U.K.
[60] School of Physics and Astronomy, University of Glasgow, Glasgow, U.K.
[61] Oliver Lodge Laboratory, University of Liverpool, Liverpool, U.K.
[62] Imperial College London, London, U.K.
[63] Department of Physics and Astronomy, University of Manchester, Manchester, U.K.
[64] Department of Physics, University of Oxford, Oxford, U.K.
[65] Massachusetts Institute of Technology, Cambridge, MA, U.S.A.
[66] University of Cincinnati, Cincinnati, OH, U.S.A.
[67] University of Maryland, College Park, MD, U.S.A.
[68] Los Alamos National Laboratory (LANL), Los Alamos, NM, U.S.A.
[69] Syracuse University, Syracuse, NY, U.S.A.
[70] Pontifícia Universidade Católica do Rio de Janeiro (PUC-Rio), Rio de Janeiro, Brazil, associated to [3]
[71] Universidad Andres Bello, Santiago, Chile, associated to [51]
[72] School of Physics and Electronics, Hunan University, Changsha City, China, associated to [8]
[73] Guangdong Provincial Key Laboratory of Nuclear Science, Guangdong-Hong Kong Joint Laboratory of Quantum Matter, Institute of Quantum Matter, South China Normal University, Guangzhou, China, associated to [4]
[74] Lanzhou University, Lanzhou, China, associated to [5]
[75] School of Physics and Technology, Wuhan University, Wuhan, China, associated to [4]
[76] Henan Normal University, Xinxiang, China, associated to [8]
[77] Departamento de Fisica, Universidad Nacional de Colombia, Bogota, Colombia, associated to [16]
[78] Ruhr Universitaet Bochum, Fakultaet f. Physik und Astronomie, Bochum, Germany, associated to [19]
[79] Eotvos Lorand University, Budapest, Hungary, associated to [49]
[80] Faculty of Physics, Vilnius University, Vilnius, Lithuania, associated to [20]
[81] Van Swinderen Institute, University of Groningen, Groningen, Netherlands, associated to [38]
[82] Universiteit Maastricht, Maastricht, Netherlands, associated to [38]
[83] Tadeusz Kosciuszko Cracow University of Technology, Cracow, Poland, associated to [41]
[84] Universidade da Coruña, A Coruña, Spain, associated to [46]
[85] Department of Physics and Astronomy, Uppsala University, Uppsala, Sweden, associated to [60]
[86] Taras Schevchenko University of Kyiv, Faculty of Physics, Kyiv, Ukraine, associated to [14]
[87] University of Michigan, Ann Arbor, MI, U.S.A., associated to [69]
[88] Ohio State University, Columbus, U.S.A., associated to [68]

[*] Corresponding author
[a] Centro Federal de Educacão Tecnológica Celso Suckow da Fonseca, Rio De Janeiro, Brazil
[b] Department of Physics and Astronomy, University of Victoria, Victoria, Canada
[c] Center for High Energy Physics, Tsinghua University, Beijing, China
[d] Hangzhou Institute for Advanced Study, UCAS, Hangzhou, China
[e] LIP6, Sorbonne Université, Paris, France
[f] Lamarr Institute for Machine Learning and Artificial Intelligence, Dortmund, Germany

JHEP10(2025)173

[g] Universidad Nacional Autónoma de Honduras, Tegucigalpa, Honduras
[h] Università di Bari, Bari, Italy
[i] Università di Bergamo, Bergamo, Italy
[j] Università di Bologna, Bologna, Italy
[k] Università di Cagliari, Cagliari, Italy
[l] Università di Ferrara, Ferrara, Italy
[m] Università di Genova, Genova, Italy
[n] Università degli Studi di Milano, Milano, Italy
[o] Università degli Studi di Milano-Bicocca, Milano, Italy
[p] Università di Modena e Reggio Emilia, Modena, Italy
[q] Università di Padova, Padova, Italy
[r] Università di Perugia, Perugia, Italy
[s] Scuola Normale Superiore, Pisa, Italy
[t] Università di Pisa, Pisa, Italy
[u] Università della Basilicata, Potenza, Italy
[v] Università di Roma Tor Vergata, Roma, Italy
[w] Università di Siena, Siena, Italy
[x] Università di Urbino, Urbino, Italy
[y] Universidad de Ingeniería y Tecnología (UTEC), Lima, Peru
[z] Universidad de Alcalá, Alcalá de Henares, Spain
[aa] Facultad de Ciencias Fisicas, Madrid, Spain
[†] Deceased

JHEP10(2025)173